J. Physiol. (1983), **343**, *pp.* 161–196
With 15 text-figures
Printed in Great Britain

MEASUREMENT AND MODIFICATION OF FREE CALCIUM TRANSIENTS IN FROG SKELETAL MUSCLE FIBRES BY A METALLOCHROMIC INDICATOR DYE

BY L. KOVACS*, E. RIOS AND M. F. SCHNEIDER

From the Department of Physiology, University of Rochester, School of Medicine and Dentistry, 601 Elmwood Avenue, Box 642, Rochester, NY 14642, U.S.A.

(*Received 3 November 1983*)

SUMMARY

1. Myoplasmic free calcium transients were monitored with the metallochromic indicator dye Antipyrylazo III (AP III) in single frog skeletal muscle fibres cut at both ends, stretched so as to minimize or eliminate contractile filament overlap and voltage clamped using a double-Vaseline-gap system (~6 °C).

2. The dye entered the central fibre segment by diffusion from the solution applied to the two cut ends. The diffusion coefficient of AP III was about 20 times lower in the fibre than in solution. This very slow diffusion was not due to binding of dye since the ratio of bound to free dye obtained from analysis of the diffusion was only about 0·45.

3. For a given depolarizing pulse, the ratio of dye-related absorbance changes ΔA at 720 and 550 nm was the same as that produced on adding calcium to dye in calibrating solution, indicating that these signals were due to changes in myoplasmic calcium.

4. The ΔA signals at 700 or 720 nm were used to monitor transient changes in concentration of calcium–dye complex [CaD_2] and of free calcium [Ca] in the myofilament space.

5. By applying the same pulse at different times during dye entry, it was observed that increasing dye concentrations $[D]_T$ produced the following effects: (a) [CaD_2] was increased; (b) [Ca] was decreased at early times during a pulse; (c) a declining phase of [Ca] observed at late times during pulses was decreased and finally reversed to a slow rising phase at high $[D]_T$; (d) the decay of [Ca] after the pulse was slowed.

6. Analyses of the effects of $[D]_T$ on (a) the magnitude of [CaD_2] at a given early time during the calcium release produced by pulses to a given voltage and on (b) the time constant for [Ca] decay after a pulse were both consistent with a calcium:dye stoichiometry of 1:2 in the fibre as found in calibrating solution.

7. Analysis of the effect of $[D]_T$ on the [Ca] decay time constants also revealed the presence of intrinsic rapidly equilibrating myoplasmic calcium binding sites and provided the basis for obtaining estimates of the combined concentration [Ca]* of

* Present address: Department of Physiology, Medical University of Debrecen, H-4012 Debrecen, Hungary.

free calcium plus calcium bound to such sites. Unlike the estimates of [Ca], these estimates of [Ca]* are independent of the value of the calcium–dye dissociation constant.

8. As $[D]_T$ increased, there was a reciprocal increase of $[CaD_2]$ and decrease of [Ca]* at a given early time during the calcium release produced by pulses to a given voltage, so that $[CaD_2]+[Ca]^*$ was approximately constant. This is as expected for calcium release being independent of $[D]_T$ and for $[CaD_2]+[Ca]^*$ corresponding to the total released calcium at times early during release.

9. Simulations with a simplified compartmental model for redistribution of intracellular calcium demonstrated that the concept of an expansion of the effective myoplasmic volume for calcium due to the presence of the dye could be sufficient to explain all observed modifications of the [Ca] transients by the dye.

10. It is concluded that AP III at relatively low concentrations is a practical monitor of minimally modified calcium transients, whereas the modifications produced by higher dye concentrations can provide useful information about properties of both the dye in the fibre and the fibre itself.

INTRODUCTION

Skeletal muscle fibres are transformed from an inactive to an active mechanical state as a result of calcium binding to regulatory sites on thin filament troponin molecules. The calcium that performs this activating role is released from the sarcoplasmic reticulum (s.r.) into the myofilament space as a result of depolarization of the transverse tubules. The measurement of myoplasmic free calcium transients is thus of great interest for studies both of myofilament activation and of the control of calcium release.

Two general approaches to monitoring myoplasmic free calcium transients involve optical recording after introduction into the myoplasm of either metallochromic calcium indicator dyes or photoproteins having calcium-dependent luminescence (reviewed by Blinks, Weir, Hess & Prendergast, 1982). The photoproteins are relatively more slowly reacting and have a stoichiometry involving more than one calcium per photo-emitting event (Blinks, 1978), which may somewhat complicate interpretation of their emitted light signal. The metallochromic indicators are generally more rapidly reacting and are first order in calcium in some but perhaps not all cases (Thomas, 1979; Rios & Schneider, 1981*a*; Palade & Vergara, 1981). Since photoproteins involve an emission rather than an absorbance change, they can be used to record calcium transients in contracting fibres with little interference from artifacts of fibre movement. With metallochromic indicators, fibre movement causes major artifacts and must be avoided or eliminated.

The metallochromic indicator dye Antipyrylazo III (AP III) is convenient for use with our cut single skeletal muscle fibre preparations (Kovacs & Schneider, 1978; Kovacs, Rios & Schneider, 1979) because it diffuses into the fibre from the cut ends (Kovacs *et al.* 1979; Kovacs & Szucs, 1980; Palade & Vergara, 1982). Arsenazo III, another metallochromic indicator which has been used for monitoring myoplasmic calcium transients in both intact (Miledi, Parker & Schalow, 1977; Baylor, Chandler

& Marshall, 1982*b*) and cut (Palade & Vergara, 1982) fibres, has been introduced by microinjection. In this paper we present calcium transients recorded using AP III in voltage-clamped single muscle fibres stretched so as to eliminate contractile movement.

In addition to presenting calcium transients and the AP III calibrations necessary for their quantitation, we consider how the presence of the dye itself modifies the calcium transient due to its calcium-buffering action (Rios & Schneider, 1981*b*, 1982). Such dye effects need to be taken account of when interpreting calcium transients recorded with metallochromic indicators in any cell, but have not been previously analysed in detail. In this paper we show that careful assessment of the effects of dye concentration on various aspects of the calcium transient can be used to provide information regarding both the calcium:dye stoichiometry inside a cell and the intrinsic intracellular buffers for calcium. Using this approach, we present evidence that the calcium:AP III stoichiometry is 1:2 in muscle fibres, as was previously found in calibrating solutions (Rios & Schneider, 1981*a*).

Abstracts concerning various aspects of this work have been presented previously (Rios & Schneider, 1981*b*, 1982).

METHODS

Fibre preparation and experimental chamber

The procedures for preparing and mounting isolated cut segments of skeletal muscle fibres were generally similar to those used by Kovacs & Schneider (1978), except where modification was required for the double-gap system used in the present experiments. Ileofibularis or semitendinosus muscles were isolated from frogs (*Rana pipiens*) maintained at room temperature and fed on crickets. The muscles were dissected down to a thin layer of fibres in Ringer solution. The solution bathing the preparation was then changed to a high potassium, calcium-free 'relaxing' solution. Following relaxation from the resulting potassium contracture, a single fibre was isolated for a distance of about 1–1·5 cm and cut at both ends.

The cut fibre was transferred to a double-Vaseline-gap chamber milled in lucite. The chamber (Fig. 1) consisted of three pools separated by two walls about 300 μm wide. The length of the middle pool was adjustable; it was set at 700 μm in most experiments. A small groove in the top surface of each wall ran from one pool to the next. For fibre mounting the two grooves were partially filled with Vaseline and the chamber was filled with excess relaxing solution so that the walls separating the pools were covered by solution. The fibre segment was mounted so as to run from one end pool to the other, spanning the length of the middle pool, via the grooves as shown in Fig. 1. Both cut ends were clamped to movable blocks in the end pools. By sliding the blocks away from the middle pool, the fibre was stretched to a sarcomere length that was generally in the range of 3·4–4 μm in these experiments. To minimize the diffusion distance and impedance of the fibre segments in the end pools, several notches were cut in the fibre in the end pools as close as possible to the partition walls (Fig. 1).

The space around the fibre in the grooves was filled with Vaseline and the upper surface of the partition walls was covered with Vaseline. A lucite 'covering' piece was placed on each wall so that its edge was even with the side of the wall facing the middle pool. As shown in Fig. 1, the covering pieces were shaped so as to extend the middle compartment toward the end compartments above the partition wall. This was necessary to accomodate the water immersion objective used in the optical measurements. After positioning these covering pieces the relaxing solution in the end pools was replaced by the 'internal' solution that contained the metallochromic indicator dye Antipyrylazo III. The chamber was then clamped to a movable stage in the experimental set up. All aspects of fibre dissection and mounting were carried out at room temperature.

Solution composition

Ringer solution: 115 mM-NaCl, 2·5 mM-KCl, 1·8 mM-$CaCl_2$, 1 mM-Na Tris-maleate buffer.

Relaxing solution: 120 mM-potassium glutamate, 2 mM-$MgCl_2$, 0·01 mM-EGTA, 5 mM-Na Tris-maleate buffer.

External solution: 75 mM-$(TEA)_2SO_4$, 5 mM-Cs_2SO_4, 7·5 mM-total $CaSO_4$, 5 mM-Na Tris-maleate buffer, 10^{-7} g/ml. tetrodotoxin.

Internal solution: 108 mM-glutamic acid, 108 mM-CsOH, 5·5 mM-$MgCl_2$, 5 mM-ATP, 1 g/l. glucose, 4·5 mM-Na Tris-maleate buffer, 13·2 mM-Cs Tris-maleate buffer, 0·1 mM-EGTA and 0·0082 mM-total added $CaCl_2$. In addition, the solution contained the dye Antipyrylazo III (ICN K & K Laboratories Inc., Plainview, NY) at concentrations ranging from 0·3 to 1·5 mM. ATP and glucose were added

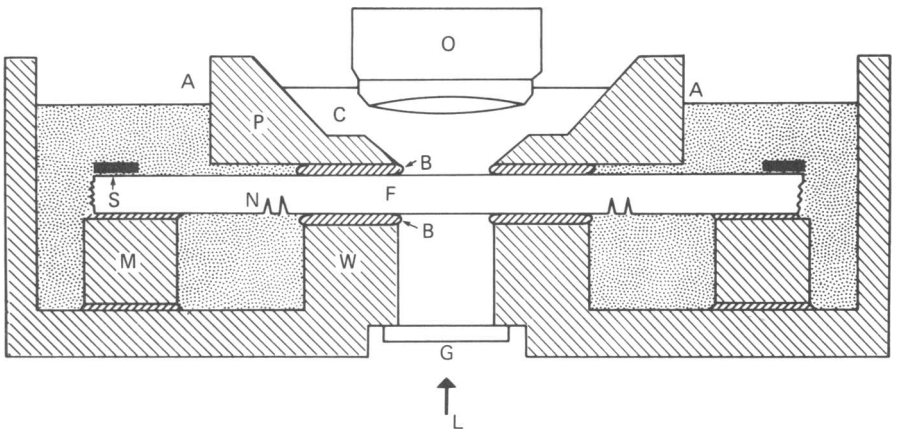

Fig. 1. Diagrammatic representation of a cut fibre mounted in the experimental chamber. A vertical section through the middle of the chamber is illustrated. F, muscle fibre; A, end pools, containing 'internal' solution that includes the dye Antipyrylazo III; C, middle pool; W, walls separating pools, with groove for accomodating the fibre; B, Vaseline seals between fibre and walls, and between fibre and covering pieces; P, covering pieces placed above the partition walls; N, notches cut in fibre; M, movable blocks; S, pieces of Scotch tape for holding ends of fibre segment to the moveable blocks; G, glass cover-slip used as chamber floor below fibre in middle pool; O, water immersion objective; L, incident beam of light.

just before the experiment and the pH set to 7·0 using CsOH. The free calcium concentration of the internal solution was $4{\cdot}34 \times 10^{-8}$ M assuming a dissociation constant for EGTA-Ca of $4{\cdot}9 \times 10^{-7}$ M, as calculated according to Harafuji & Ogawa (1980). The free magnesium concentration was 0·94 mM, using a value of 9×10^{-5} M for the Mg ATP dissociation constant (Fabiato & Fabiato, 1975).

Calibration solution: 93 mM-glutamic acid, 108 mM-CsOH, 4·5 mM-Na Tris-maleate buffer, 13·2 mM-Cs Tris-maleate buffer, 15 mM-HEDTA, 1 g/l. glucose, 0·05, 0·1875, 0·75, 1·00 or 1·449 mM-Antipyrylazo III, various concentrations of total added $CaCl_2$.

The pH of all solutions was adjusted to 7·0 at room temperature.

Electrical measurements and analog electronics

The electrical connexions to the chamber are shown schematically in Fig. 2. The voltage difference V_P between one of the end pools (called hereafter the voltage pool) and the middle pool was recorded using two agar bridges and unity-gain voltage followers, followed by a differential amplifier (amplifiers A1–3, Fig. 2). The middle pool was held at virtual ground using two other agar bridges and amplifier A4. The total current applied to the fibre was monitored as the voltage drop across the resistor R_I by amplifer A6. Amplifier A5, in potentiometric configuration, prevented any fibre current flow through the input of A6. The other end pool (the current pool) was connected

either to a voltage source E_P or to the output of a voltage-clamp amplifier (A8) via a fifth agar bridge and a switch. Agar bridges contained 2% agar either in internal solution without ATP and glucose for the end pools or in external solution for the middle pool. Each bridge contacted a 3 M-potassium chloride pool fitted with silver/silver chloride pellet electrode.

For initial electrical checks the current pool was connected to E_P, which applied 22 mV pulses from a steady level of 0 mV. and the resulting change in V_P was monitored. At this stage of the

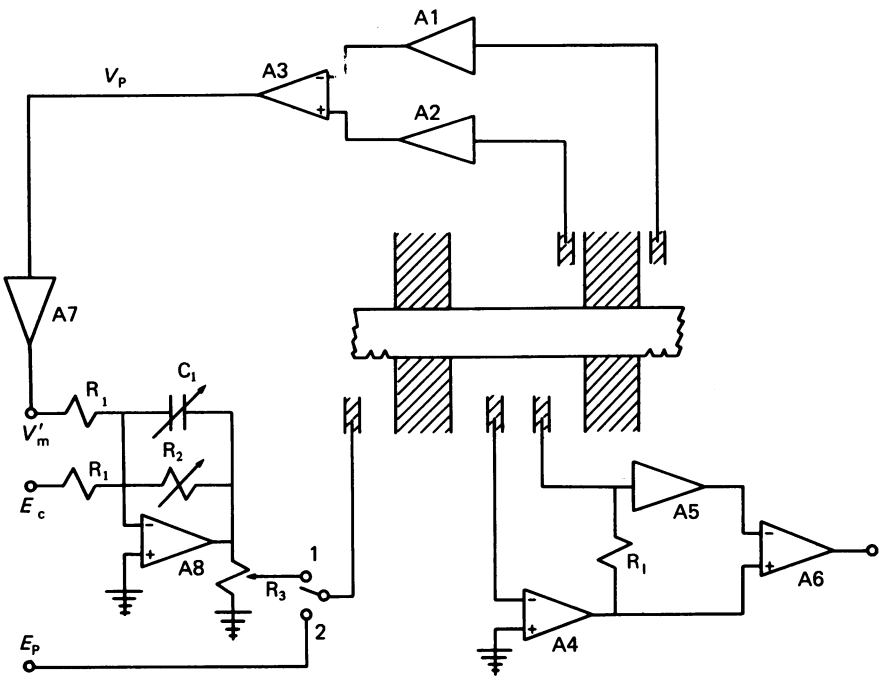

Fig. 2. Voltage and current recording circuits and voltage control circuit. Amplifiers A1–A3 measured the voltage difference between one of the end pools and the middle pool. A1 and A2 were unity gain FET input voltage followers and A3 was a unity gain differential amplifier having a time constant of 10^{-7} sec. The pool voltage difference V_P, measured by A3, was proportional to the transmembrane voltage in the middle pool, V_m, reduced by the gap attenuation factor. After estimating the gap factor as described in the text, the gain of amplifier A7 was adjusted to compensate for the gap attenuation. Its output V'_m, considered to be a measure of V_m, was controlled by the voltage clamp amplifier A8 to equal $-E_c$ when the switch was in position 1. Position 2 of the switch was used for applying voltage E_P directly to the current-passing pool. A4 was connected in currentometric configuration using two agar bridges so as to hold the middle pool at virtual ground. The total current entering the pool was monitored by A6, a unity gain differential amplifier (time constant of 10^{-5} sec), as the voltage drop across R_I (100 kΩ). A5, a unity gain FET input follower, isolated the pool from amplifier A6. A1–A7 were made using Signetics 536 operational amplifiers connected in standard feed-back configurations. The control amplifier A8 was a Teledyne–Philbrick 1434 with $R_1 = 10$ kΩ, $10\ \text{kΩ} \leqslant R_2 \leqslant 10$ MΩ, $R_3 = 1{\cdot}1$ kΩ and $30 \leqslant C_1 \leqslant 3000$ pF.

procedure, when the steady change in V_P was greater than about 60% of E_P the quality of the seals was considered adequate. The middle pool was then changed to the 'external' solution, the chamber was moved so as to position the fibre in the light path, an electrically isolated water immersion objective was lowered to touch the solution in the middle pool and the chamber was cooled using a Peltier device (Cambion, Cambridge, MA). When the temperature reached a steady value of between 6 and 9 °C the electrical properties of the fibre were carefully assessed. In many

experiments, micro-electrode measurements of the actual transmembrane potential of the fibre segment in the middle pool were obtained at this stage and indicated that the applied 22 mV E_P pulse produced a steady transmembrane voltage change of about 20 mV in the middle compartment during the pulse. In view of this reproducibility, the magnitude of the attenuation factor for the gap-recorded membrane voltage was estimated to equal $V_P(\infty)/20$, where $V_P(\infty)$ was the steady value of the voltage change across the Vaseline-gap for voltage recording. Its value at this stage was usually between 0·8 and 1·0. The adjustable gain of amplifier A7 was set to $20/V_P(\infty)$, so that its output was now approximately equal to the membrane voltage in the middle portion of the fibre. This was the signal fed back to the clamp amplifier A8. The membrane voltage was then clamped by connecting the current pool to the output of A8. The holding potential was taken rapidly to −90 mV and the fibre was allowed to reprime at this potential for 15 min before starting data acquisition. When the actual recording started, the fibres had usually been exposed to the dye-containing internal solution for about 45 min.

Temperature was routinely monitored using a thermistor mounted at the edge of the middle pool, about 1 cm from the fibre. Due to the central hole for light passage through the cooling device and the heat sink effect of the water immersion objective above the fibre, the temperature at the fibre was several degrees warmer than that monitored. A second small thermistor mounted on a micromanipulator and positioned within 100 μm of the fibre was used in a few experiments. Comparison of the two readings was used to correct all routinely monitored temperatures to temperatures at the level of the fibre, which were 6–9 °C in these experiments. This was also the actual range of temperatures at the fibre in our earlier experiments, rather than the previously reported range of 2–4 °C (Kovacs *et al.* 1979; Schneider *et al.* 1981) which was not corrected for the temperature difference.

Optical measurements

Aspects of the set-up relevant to the optical measurements have been briefly described previously (Kovacs & Schneider, 1977) and are represented in Fig. 3. The chamber was clamped to a movable stage that served a compound microscope with nosepiece focusing (American Optical, Microstar). The stage was supported independently of the microscope, which was itself incorporated into an optical rail arrangement. Light from a 100 W tungsten-halogen bulb powered by a 12 V battery was focussed by lenses L_1 and L_2 on an adjustable slit about 3 mm long by 0·8 mm wide. The bulb was mounted in a commercial lamp housing (Oriel) that was modified to minimize air currents. The band width of the incident light was established by a filter placed between the slit and the fibre. In the earlier exeriments 10 nm half-peak band width interference filters (Ditric Optics; Oriel) were used for characterizing the wave-length dependence of the signals. In later experiments, broadband interference filters (Oriel, no. 5763, 5769) that gave better signal-to-noise ratios were used. A long working distance objective (10 ×, 0·25 N.A. Nikon 77795), used as a condenser, sent the light through a glass cover-slip in the chamber floor, forming a reduced size image of the slit in the centre of the fibre. The length of the slit image was about 250 μm and its width was adjusted so as to occupy about 80% of the fibre width (50–120 μm). A water immersion objective (40 ×, 0·75 N.A., Zeiss 561702) collected the transmitted light for either binocular observation or intensity measurement.

For photometry, the fibre image made by the objective was relayed by a lens to a photodiode (Electro-Nuclear PDS-050GB) located in the trinocular tube of the microscope. The photodiode was connected to an operational amplifier circuit in a photoconductive configuration. The voltage output of this circuit, proportional to the light inensity on the photodiode, was monitored using a high-gain amplifier (Tektronix 3A9 vertical amplifier in a 565 oscilloscope). In order to detect very small changes in the high intensity light beam with sufficient resolution, it was necessary to electronically cancel the signal due to the steady light component. In the earlier experiments (fibre numbers up to and including B96), this was accomplished by using the low frequency input cut-off filter on the 3A9 amplifier at a setting of 0·1 Hz. The minor distortion introduced by such single time constant filtering was removed numerically from the recorded transient signals during data processing. In all later experiments the output V_I of the photocurrent amplifier was first fed to a track and hold stage (Vergara, Bezanilla & Salzberg, 1978). Then both V_I and the track and hold output were connected differentially to the high-gain amplifier (3A9) operating without low frequency cut-off. The track and hold circuit was gated so that during each pulse it held the voltage corresponding to the light intensity just before the pulse, thus providing a reference level for the measurement of the change in intensity due to the pulse. In both cases the high frequency cut-off

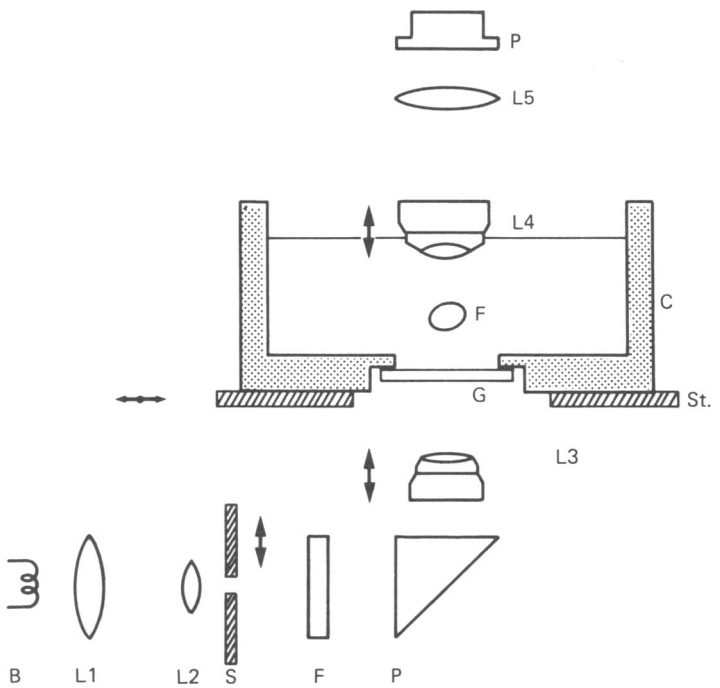

Fig. 3. Optical system for monitoring light transmitted by a muscle fibre. The light source B, a 100 W tungsten–halogen bulb powered by a 12 V mine car battery, was mounted in a commercial housing (Oriel Corporation, Stamford, CT) that included lens L1. A real 1 × image of the filament was formed by L1 near the first focal plane of component L2, a pair of contiguous lenses of 18 mm diameter and 20 mm focal length (Edmund Scientific Co., Barrington, NJ). The roughly collimated beam from L2 illuminated the adjustable slit S. An interference filter F (either 10 nm half-peak band width filter from Ditric Optics, Inc., Marlboro, MA or a 70 nm half-peak band width filter from Oriel Corp., Standford, CT) established the spectrum of the incident light, which entered a trinocular microscope (American Optical, Buffalo, NY) after total reflexion in prism P. The condenser L3 was a long working distance microscope objective (10 ×, 0·25 NA, Nikon 77795) used in inverted configuration to form a 10 × reduced focused image of the slit in the centre of the fibre, F. The fibre was mounted in the experimental chamber, C, shown here in vertical section perpendicular to the vertical section in Fig. 1, with central floor made of a glass cover-slip, G. The chamber was mounted on a movable stage, St., that allowed positioning of the fibre in or out of the illuminating light beam. The water immersion objective, L4 (40 × 0·75 N.A., Zeiss 561702) formed an internal image of the illuminated fibre, which in turn was reduced in size and projected by L5 (a 1″ diameter, 50 mm focal length plano convex lens; Edmund Scientific) on the active surface of the photodiode, P (Electro-Nuclear PDS-050GB). Both L5 and the photodiode were located in the trinocular tube of the microscope and positioned so as to form a sharp image of the slit on the photodiode surface when the microscope was well focused for binocular observation. Arrows indicate component movements carried out during an experiment to set the slit width, focus the slit image on the fibre, position the fibre relative to the beam and focus the fibre image. Positions of all other elements, including those of the microscope, were fixed by mounting on a home-made optical rail.

of the 3A9 amplifier was set at 1 kHz. Steady values of V_I of resting fibres were monitored by using a d.c.-coupled digital voltmeter (Fluke 8000A).

The sarcomere length s of each fibre was determined using the microscope with a filar micrometer eyepiece (American Optical) to measure the total length of ten sarcomeres.

Data acquisition and preliminary signal processing

A voltage time course $\Delta V_I(t)$ proportional to the change $\Delta I(t)$ in transmitted light intensity from its reference level was recorded on-line by a minicomputer system. Occasionally, the pool voltage or total current were recorded also. The fundamentals of the recording procedure have been described elsewhere (Chandler, Rakowski & Schneider, 1976; Kovacs & Schneider, 1978). Briefly, a voltage-to-frequency converter and a counter performed the analog-to-digital conversion. Their output was a sequence of integrals of the signal in successive time intervals. These integrals were sent to a small laboratory computer (Digital Equipment Corporation, PDP 8-E) where records of successive pulses could be averaged. The average records were stored on floppy disks for subsequent processing.

Following an experiment records of absorbance change time courses, $\Delta A(t)$, were calculated from the V_I data. The definition of $\Delta A(t)$ is given by

$$\Delta A(t) = \log_{10}\{I_0/[I+\Delta I(t)]\} - \log_{10}\{I_0/I\}, \quad (1)$$

where I_0 is the incident light intensity, I the intensity of light transmitted in the reference condition and $\Delta I(t)$ the time course of light intensity change from the reference condition. Rearranging eqn. (1) to eliminate I_0, noting that I and ΔI are proportional to V_I and ΔV_I and converting to natural logarithms gives

$$\Delta A(t) = 0{\cdot}43 \ln\{V_I/[V_I+\Delta V_I(t)]\}. \quad (2)$$

For $\Delta V_I \ll V_I$, which was generally the case in these experiments, eqn. (2) can be approximated by

$$\Delta A(t) = -0{\cdot}43\, \Delta V_I(t)/V_I, \quad (3)$$

so that the absorbance change was approximately proportional to the recorded voltage change. All results in the present report were obtained using the exact eqn. (2).

Determination of dye concentration

In order to interpret ΔA signals in terms of changes in concentration of free and dye-reacted calcium, it was necessary to know the total dye concentration $[D]_T$ and the stoichiometry, molar extinction coefficient change and dissociation constant for the calcium:dye reaction. The dye concentration in the fibre was estimated according to

$$[D]_T = [A_{550} - (790/550)\, A_{790}]/(0{\cdot}7\, p\epsilon_{550}), \quad (4)$$

where A_{550} and A_{790} are the absorbances of the resting fibre at 550 and 790 nm, p is the length of the light path through the fibre, 0·7 is an approximate estimate of the fraction of the path occupied by aqueous solution accessible to the dye and ϵ_{550} is the molar extinction coefficient of the dye at 550 nm. The term $(790/550)\, A_{790}$ is an estimate of the relatively small non-dye-related intrinsic 'absorbance' of the fibre at 550 nm. It is obtained from the fibre absorbance at 790 nm, a wave-length at which the dye exhibits no light absorbance, assuming the intrinsic absorbance of the fibre to vary inversely with wavelength (Baylor *et al.* 1982*a*). The value of p for each estimate of $[D]_T$ was obtained by focusing the microscope on the upper and lower surfaces of the fibre and taking the difference in readings of the microscope calibrated fine focus knob. In earlier experiments (fibre numbers up to and including B62), p was not directly measured. For these fibres p was assumed to equal the fibre width d in the plane perpendicular to the microscope axis.

Calibration of the calcium–antipyrylazo III reaction

We have previously presented values for the extinction coefficient change, dissociation constant and stoichiometry of the calcium–Antipyrylazo III reaction in a predominantly potassium chloride solution at room temperature (Rios & Schneider, 1981*a*). In an attempt to obtain estimates that may be closer to the values of these parameters inside the fibre in our experiments, we re-examined the reaction in the predominantly caesium glutamate 'calibration' solution at 5 °C using the previously described procedures (Rios & Schneider, 1981*a*).

The composition of the 'calibration' solution used for the dye calibration measurements was given

in a previous section. Its only differences from the 'internal' solution used in the fibre experiments were (i) no EGTA and no ATP were added; (ii) the total magnesium concentration was 0·5 mM; (iii) 15 mM of the glutamic acid of the 'internal solution was replaced by the calcium buffer HEDTA (*N*-2-hydroxyethyl ethylenedinitrilo-*N*,*N*′,*N*′-triacetic acid). Calibrations were carried out in this solution at dye concentrations of 50, 187·5 and 750 μM, which are identical to those in our previous measurements (Rios & Schneider, 1981*a*), using a Spectronic 100 spectrophotometer (Bausch and Lomb, Inc.) in a cold room at 5 °C. The results are presented in Fig. 4. The ordinate of the plot

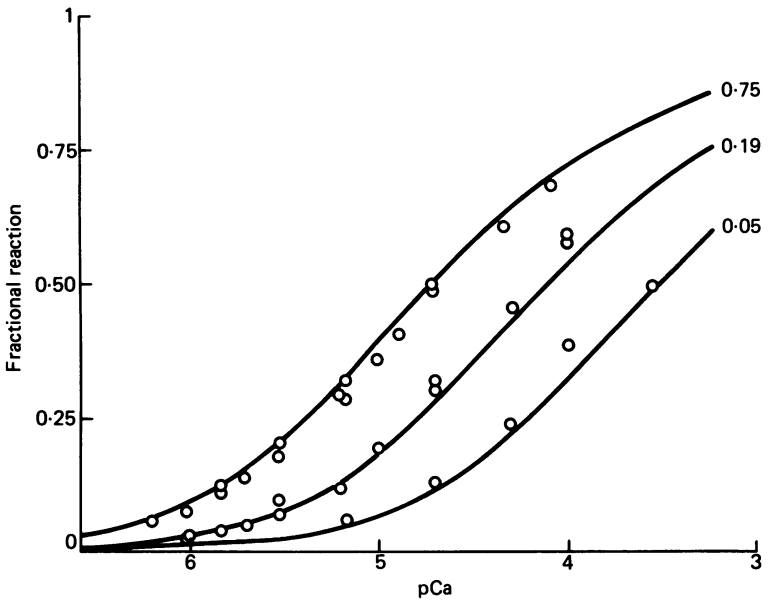

Fig. 4. Calibration of AP III absorbance changes. Absorbance changes at 720 nm upon addition of $CaCl_2$ to the calibration solution given in the text. The three sets of points correspond to three different dye concentrations: 0·05, 0·1875 and 0·75 mM in 1, 0·2 or 0·1 cm cuvettes. The raw data, total calcium concentration, total dye concentration and ΔA were the input to a computer program described by Rios & Schneider (1981*a*). The program used an iterative, non-linear least-squares routine to fit the data with the theoretical dependence of a 1:2 calcium:dye reaction. Two parameters specify this model: the differential extinction coefficient $\Delta\epsilon$ and the dissociation constant K_D. If the fit converged, in addition to estimates of these parameters the program also calculated the value of free calcium concentration [Ca] and fractional reaction of the dye corresponding to each measurement, which are the coordinates of the points in this plot. The curves represent the best fit theoretical dependence. The best fit parameter values were: $\Delta\epsilon = 8{\cdot}2 \times 10^3 \pm 0{\cdot}25\ M^{-1}\ cm^{-1}$ and $K_D = 13131 \pm 1039\ \mu M^2$. Standard error of fit = 0·008.

is the fraction of dye reacted with calcium at the free calcium concentration given on the abscissa in logarithmic scale. The theoretical dependence for a given calcium:dye stoichiometry was simultaneously fit to the data obtained at all three different dye concentrations. The fitting was carried out by an iterative non-linear least-squares method that used the total calcium added and the corresponding absorbance increase at each point as input data. The program then derived the best fit reaction parameters as well as the fractional reaction and the free calcium concentration [Ca] corresponding to each point from the input data and the specified stoichiometry (Rios & Schneider, 1981*a*). The continuous lines in Fig. 4 represent the best fit theoretical dependence for the 1:2 calcium:dye stoichiometry. The results correspond quite closely to the 1:2 stoichiometry relationship in this range of concentrations. The best fit parameters are given in the Figure legend. The maximum change in absorbance was exactly the same as that found previously at room

temperature in potassium chloride, whereas the dissociation constant, 13,100 μM^2, was three times smaller than the value of 40,000 μM^2 measured previously (Rios & Schneider, 1981*a*). In order to decide whether the higher affinity under the present conditions of calibration (low temperature, solution containing caesium glutamate) was due to the different temperature or the different main ions in the solution, we carried out calibrations at room temperature in the caesium glutamate 'calibration' solution. Again the data were fit very well with the theoretical dependence of a 1:2 stoichiometry. The best fit parameters were 25,500 μM^2 for the dissociation constant and 0·330 for

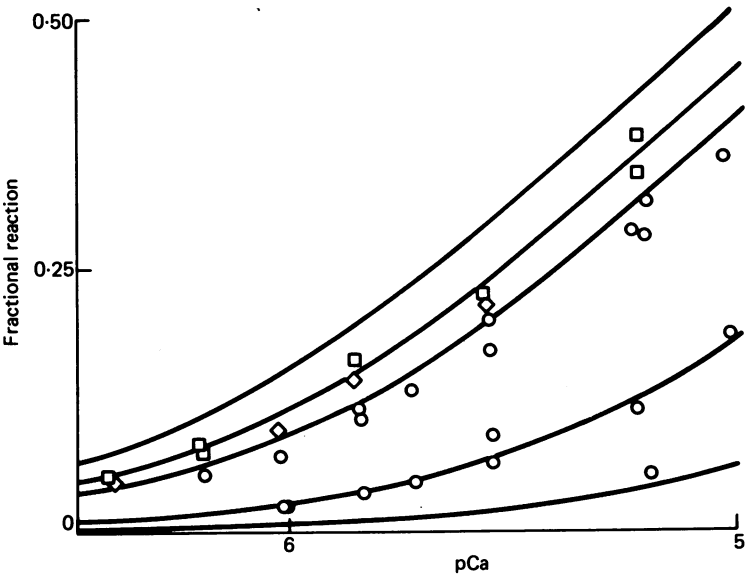

Fig. 5. Calibration at high AP III concentrations. Data obtained in the same way as for Fig. 4; only the range of [Ca^{2+}] $\leqslant$ 10 μM and fractional reaction $\leqslant$ 0·5 is shown. The circles are identical to the points in Fig. 4 that lay within this range. Results at higher dye concentrations are also shown: (◇) at [dye] = 1·00 mM; (□) at [dye] = 1·449 mM. The lines correspond to the theoretical dependence for 1:2 stoichiometry with the same values of the parameters as in Fig. 4. The Figure illustrates systematic deviations from the model at high dye concentrations.

the normalized maximum absorbance change. Thus, part of the increase in affinity was due to substituting caesium glutamate for KCl and an additional increase was due to the lower temperature. The maximum absorbance change remained remarkably constant, indicating that there were no changes in the extinction coefficient of the free or the calcium-bound dye at this wave-length with these changes in calibration conditions.

In the present calibrations, the level of free magnesium was kept well below 10^{-4} M by the presence of HEDTA. The 'internal' solution applied to the cut fibre ends in our muscle experiments had a free Mg concentration of 0.94 mM (above). The effect of free magnesium on the calcium–dye reaction is to increase the calcium–dye dissociation constant, in this case by a factor calculated from the equations of Rios & Schneider (1981*a*) to be 1·33 for an assumed free magnesium concentration of 1 mM inside our cut muscle fibres. After correction for magnesium the dissociation constant becomes 17,500 μM^2, the value used in all the subsequent analyses of the fibre results. In this calculation we assumed, for simplicity, that the magnesium effect did not depend on temperature and was the same in potassium chloride and caesium glutamate.

The calcium buffer HEDTA was used to set the level of free calcium for these calibrations. Its dissociation constant for calcium was calculated from the published affinity constant at room temperature (Martell & Smith, 1974), which we adjusted to the value appropriate to 6 °C using van't Hoff's law and the value of the molar enthalpy change given by Martell & Smith (1974) for this

reaction. The published constants were determined in potassium chloride at 0·1 M ionic strength but were assumed to be valid for our calibration solution, which was essentially caesium glutamate at 0·1 M ionic strength. The calculated value for the HEDTA dissociation constant was $5{\cdot}998 \times 10^{-6}$ M.

Close examination of Fig. 4 reveals indications of a small systematic deviation of the fit from the data: the experimental points at the highest dye concentration tend to fall systematically below the theoretical curve. Additional measurements demonstrated that this discrepancy was more severe at even higher dye concentrations. Fig. 5 presents results at 1 mM (diamonds) and 1·45 mM (squares) dye concentration, as well as the data from Fig. 4 for lower dye (circles). Only the range of [Ca] below 10 μM is shown in Fig. 5. The lines correspond to the theoretical dependence calculated for 1:2 stoichiometry using the same parameters as for Fig. 4. The three lower curves are thus segments of the curves in Fig. 4. The experimental points at the two highest dye concentrations fall clearly below the corresponding two left-most theoretical curves. When the theoretical function for 1:2 stoichiometry was fit to all data for only 0·75, 1·0 and 1·5 mM dye, a good fit was obtained, although with a slightly different value of the dissociation constant. Other possible stoichiometries tested for the range of dye between 0·75 and 1·5 mM gave worse fits. It is possible that at these high dye concentrations the reaction becomes complicated by the appearance of significant amounts of products with different stoichiometries.

In view of the uncertainty regarding the calcium–dye reaction at relatively high dye concentrations, for the present paper we have used only results obtained with myoplasmic dye concentrations less than or equal to 0·75 mM. Over this range we assumed a 1:2 stoichiometry for the calcium:dye reaction with an apparent K_D of 17500 μM[2]. Quantitative interpretation of results obtained with higher dye concentrations must await further calibrations and a better understanding of the reaction in that range.

RESULTS

The absorbance spectrum of antipyryazo III in muscle fibres

The resting fibre light absorbance at a variety of wave-lengths generally was monitored several times during the course of each experiment as dye entered the central fibre segment. Assuming the intrinsic optical properties of the fibre to remain constant, differences in successive absorbance measurements would be due exclusively to changes in dye concentration and their wave-length dependence would correspond to the absorbance spectrum of AP III inside the muscle fibre. The circles in Fig. 6 present the average spectrum of intra-fibre AP III obtained in this way from forty differences in successive sets of absorbance measurements on nineteen fibres. Prior to averaging, each set of absorbance differences was first normalized to the absorbance difference at 550 nm. The unity reference level of relative absorbance is indicated by the filled circle at 550 nm in Fig. 6. The reference wave-length of 550 nm is near the peak of the AP III absorbance spectrum and is also an isosbestic point for magnesium and pH (Scarpa, Brinley & Dubyak, 1978; Baylor, Chandler & Marshall, 1982*a*). For comparison, the vertical bars in Fig. 6 give the range of four sets of relative absorbance measurements on AP III dissolved in the internal solution at about 6 °C. Although there is general agreement of the intra-fibre and solution spectra of AP III, the fibre results appear to exhibit a somewhat greater relative absorbance in the neighbourhood of 600 nm and a smaller relative absorbance near 500 nm. Such discrepancy cannot be due to a difference in calcium concentrations since that would have produced a large effect at 720 nm which was not observed (Fig. 6). It could correspond to either a lower magnesium concentration or a lower pH within the fibre than in the internal solutions (Scarpa *et al.* 1978; Baylor *et al.* 1982*a*).

The calibration solution samples for Fig. 6 were prepared on four different occasions

and measured either in a 200 μm diameter glass tube positioned in place of the muscle fibre on the experimental set up or in the commercial spectrophotometer. Surprisingly, the calibration solutions themselves exhibited considerable variability in relative absorbance in the neighbourhood of 500 and 600 nm. The origin of this variability is uncertain. It apparently was not due to random preparation or measurement errors since sets of solutions prepared in parallel on a given day all exhibited

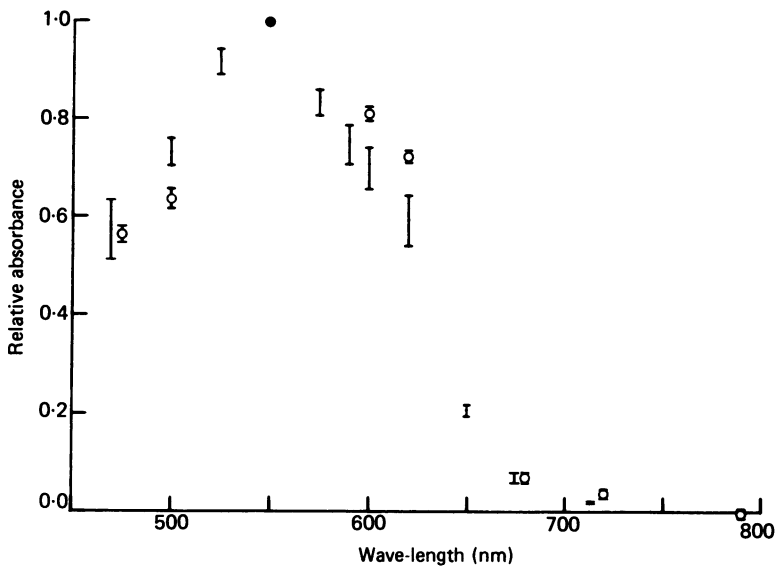

Fig. 6. Absorption spectra of the dye Antipyrylazo III in resting fibres and in the internal solution. Abscissa: wave-length. Ordinate, absorbance, relative to the absorbance at 550 nm (filled circle). ○, averages of measurements in nineteen fibres. The values averaged were differences $A(t_2)-A(t_1)$ in the absorbance at two times (t_1 and t_2) during the experiment. Three such differences, at intervals t_2-t_1 of about 30 min, were calculated in most experiments. The individual differences in all experiments were averaged with the same weight. Error bars for circles give the standard error of the mean for fibre measurements. The vertical bars give the range of four sets of relative absorbance measurements of the dye in internal solution (~6 °C). Two sets of measurements were carried out on a commercial spectrophotometer (Bausch and Lomb, Spectronic 100) using 0·6 mM-dye and 1 mm path length cuvettes. The others were carried out on the experimental set up using 1·5 mM-dye in a capillary tube (internal diameter = 220 μm) placed in the experimental chamber.

uniformly low relative absorbance near 600 nm and uniformly high absorbance near 500 nm, or vice versa. There was no systematic difference between results obtained using the spectrophotometer and the muscle fibre optical set up.

Our general conclusion is that the dye has similar absorbance spectra in muscle fibres and in the internal solution. The minor differences between the intra-fibre and solution spectra may have been caused by uncontrolled differences in medium composition.

The time course of dye entry

The dye was applied to the end pools. During the experiment it diffused into the middle portion of the fibre, where its concentration was determined as described in the Methods section. This was done at intervals of 10–20 min in the course of nine experiments in order to study the time dependence of this diffusion process, which was found to be much slower than expected.

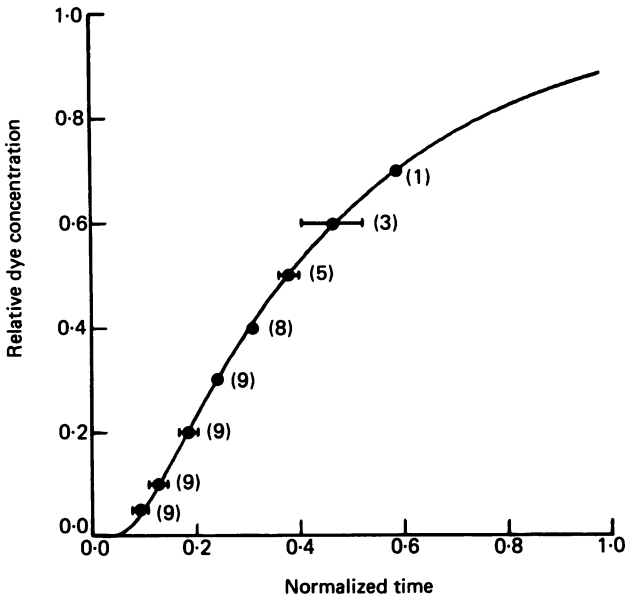

Fig. 7. Time course of dye entry. Average values for nine fibres. Ordinate: dye concentration calculated from the resting absorbance at 550 nm in the centre of a fibre and normalized to its equilibrium value. The equilibrium concentration was assumed to be 45 % higher than the concentration in the end pools, which was 1 mM in seven fibres and 1·5 mM in two fibres. Abscissa: time, normalized as described in the text, to attain each relative concentration in the ordinate. Horizontal bars give ± 1 standard deviation. The number of fibres that attained each relative dye concentration is indicated next to the symbols. The continuous curve gives the theoretical time course of relative concentration at the centre of a rod of length $2l$ with symmetric boundary concentrations. The abscissa for the curve is the dimensionless variable $\kappa t/l^2$, where κ is the diffusion constant and t is time.

The diffusion of dye in the fibres was compared with the model of one dimensional diffusion in a rod of length $2l$. In the model the concentration was initially 0 and a boundary concentration value was imposed symmetrically at both ends at time $t = 0$. The curve in Fig. 7 represents the general solution to this problem. The ordinate y is concentration relative to the boundary value; the abscissa is the dimensionless time variable $T = \kappa t/l^2$, where κ is the diffusion coefficient. The curve was generated according to Carlslaw & Jaeger (1947) by computing the first eleven terms of the series

$$y = 1-(4/\pi)\sum_{n=0}^{\infty}\{[(-1)^n/(2n+1)]\exp[-(2n+1)^2\pi^2T/4]\cos[(2n+1)\pi x/2l]\}, \quad (5)$$

where x is distance from the centre of the fibre, which was assumed to equal zero in calculating the curve in Fig. 7. The inverse of eqn. (5) gives the functional dependence of T on y, which will be henceforth referred to as $T(y)$.

For comparison with the general dimensionless solution presented in Fig. 7, the experimental results (concentration *vs.* time) from each of the nine fibres required normalization in both coordinate axes. To normalize the concentrations, the measured values were divided by the theoretical equilibrium concentrations, which would be equal to the concentration in the end pools if no binding occurred. In order to account for the observations we had to assume an equilibrium value of 1·45 times the end pool concentration.

Normalization of the abscissa consisted of converting the measured time $t(y)$ to reach any relative concentration y to the corresponding dimensionless variable $\kappa t(y)/l^2$. To accomplish such time normalization, graphs of y *vs.* t were first constructed for each fibre. By interpolation in these graphs the time to reach a set of up to the eight relative dye concentrations $y_i = 0{\cdot}05, 0{\cdot}1, 0{\cdot}2, 0{\cdot}3, 0{\cdot}4, 0{\cdot}5, 0{\cdot}6$ and $0{\cdot}7$ were determined for each fibre. If diffusion in the fibre followed the theoretical curve $T(y)$, then $\kappa t(y_i)/l^2$ would equal $T(y_i)$ and the time normalization factor κ/l^2 could be calculated as $T(y_i)/t(y_i)$, which should be independent of y_i. Following this reasoning, a time normalization factor equal to the average value of $T(y_i)/t(y_i)$ was calculated for each fibre. Each measured $t(y_i)$ value for the fibre was then multiplied by this factor. The resulting values of dimensionless time required to reach each y_i were then averaged over all fibres and are represented as circles in Fig. 7.

Comparison of the mean normalized experimental values with the theoretical curve in Fig. 7 indicates that diffusion in the fibre followed the one dimensional model acceptably well. Accordingly, the time normalization factor is an estimate of κ/l^2 for each fibre. As we do not know the value of l for each fibre due to uncertainty as to the exact location of the notches, we averaged the time normalization factor over all fibres and assumed l to equal 0·9 mm corresponding to about 300 μm each for distances from walls to illuminated region, width of the walls and distance from wall to closest notch. This resulted in an estimate of $3{\cdot}6 \times 10^{-7}$ cm^2/sec for the diffusion coefficient of the dye in our experimental conditions.

This value is much lower than expected for a molecule of the size of AP III (Hobbie, 1978) and about three times less than the value obtained by R. Rakowski (personal communication) for diffusion of the related molecule Arsenazo III in muscle fibres. Our value for κ may underestimate its actual intrafibre value to an unknown extent due to the distance to the first open notch being greater than assumed or to the dye having limited access to the fibre interior at the notch. To rule out some peculiarity of the diffusion of AP III in free solution we took measurements of diffusion of AP III in a capillary tube containing internal solution. In order to prevent turbulence, the end of the tube was occluded with a polyacrylamide gel stopper approximately 0·5 mm thick. This end of the tube was exposed to dye-containing internal solution and the time course of dye increase was measured at four points along the tube by means of our optical set up. The diffusion coefficient was derived by direct application of Fick's law and found to be $8{\cdot}3 \times 10^{-6}$ cm^2/sec.

The diffusion coefficient in the fibre is thus approximately 20 times smaller than in free solution. Considering the reports that indicate binding of the dye Arsenazo

III to cell structures (Beeler, Schibechi & Martonosi, 1980) the slow diffusion of Antipyrylazo III could be the consequence of binding. However, in order to account for a 20-fold reduction in κ a ratio of bound to free dye of 19 would be necessary (Crank, 1975). Such a degree of binding is clearly inconsistent with the observations and analysis represented in Fig. 7, which suggests a value of 0·45 for the ratio of bound to free dye. Analyses similar to that for Fig. 7 but using 0·3 or 0·6 for the value of bound/free dye deviated in opposite directions from the theoretical relationship, indicating that the actual value was probably between these limits.

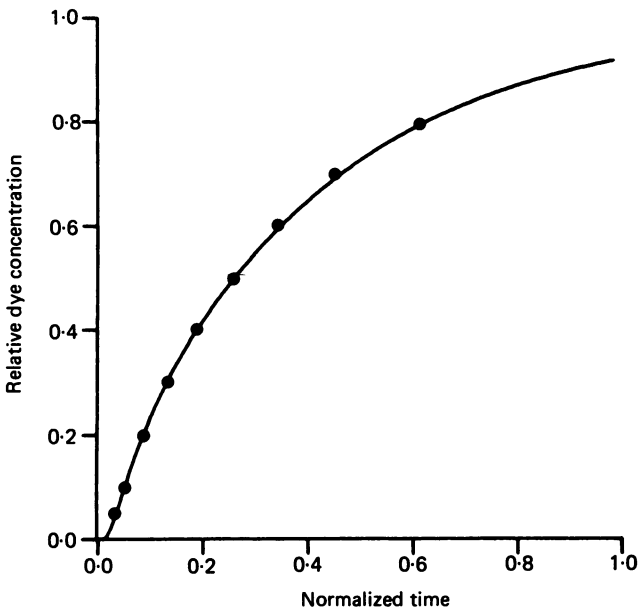

Fig. 8. Dye diffusion in a tube containing internal solution and agar. Ordinate: dye concentration calculated from the absorbance at 550 nm and normalized to its equilibrium value, which was assumed to be equal to the end pool concentration (0·6 mM). Abscissa: time, normalized as described in the text, to attain the concentrations in the ordinate. Agar concentration 0·3%. Length of tube 6·8 mm. Measurements done at 3·1 mm from closed end. Internal diameter 0·6 mm. $T \simeq 6$ °C. Curve: computer generated time course of concentration calculated according to eqn. (5) for a rod of length $2l$ under symmetric constant boundary values. The curve corresponds to a distance x from the centre of the rod such that $x/l = 3{\cdot}1/6{\cdot}8 = 0{\cdot}456$. Abscissa for theoretical curve: dimensionless variable $\kappa t/l^2$.

An alternative explanation for the slow diffusion in the fibre would be the existence of steric hindrance to the movement of dye. The importance of steric factors in the diffusion of AP III is illustrated by Fig. 8, which represents diffusion in a capillary tube containing internal solution plus agar at the relatively low concentration of 0·3%. The results were analysed in the same way as described for the fibre experiments, except that the concentration normalization in Fig. 8 assumed zero binding. From the average ratio $T(y_i)/t(y_i)$ the diffusion coefficient was found to be $2{\cdot}0 \times 10^{-6}$ cm^2/sec. The presence of agar at a low concentration is thus enough to cause a four-fold drop in the value of the diffusion coefficient without any evidence of binding.

The wave-length dependence of the absorbance change signals

If the absorbance change signals are to be used for monitoring calcium transients quantitatively, it is essential to verify that their characteristics are comparable to those of the absorbance changes associated with calcium changes in calibrating conditions. In order to avoid interference from changes in magnesium or hydrogen, the comparisons between the spectra of the absorbance change in the fibre and in calibration conditions were performed at 550 nm, 720 nm and 790 nm, i.e. wave-lengths where magnesium or hydrogen do not cause a direct change in extinction (Baylor *et al.* 1982*a*).

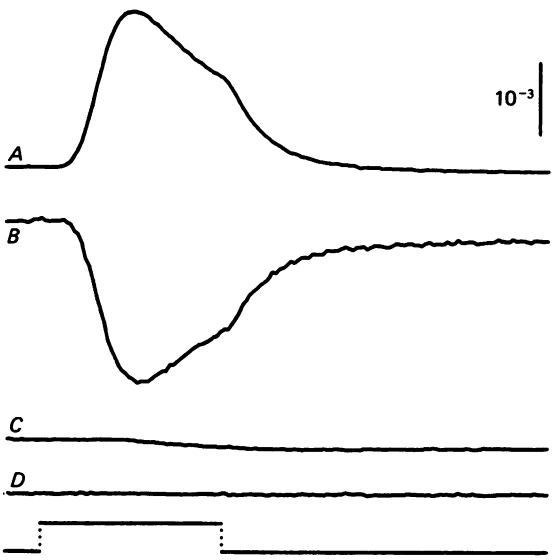

Fig. 9. Wave-length dependence of the absorbance change elicited by a depolarizing pulse. *A*, absorbance change at 720 nm. *B*, absorbance change at 550 nm. *C*, absorbance change at 790 nm. Records *A–C* are averages of two sweeps. *D*, the linear combination of *C* with scaled *A* and *B* that has the minimum sum of squared deviations from zero. $D = C - 0{\cdot}343A - 0{\cdot}349B$. The depolarizing pulse is a schematic representation of the 100 msec pulse to −30 mV. Fibre B90, sequence 4. $s = 3{\cdot}40\ \mu m$, $p = 130\ \mu m$, $[D]_T = 700\ \mu M$.

Representative records at these wave-lengths are shown in Fig. 9. As previously described (Kovacs *et al.* 1979) the signals at 720 and 550 had opposite sign, approximately the same amplitude and almost the same time course except for a small late 'off' phase which was usually a decrease in absorbance at both 720 and 550 nm. This late component cannot be due to calcium, as it had the wrong polarity at 720 nm. It was obviously an intrinsic absorbance change since, when looked for, it was observed even at the beginning of an experiment when the dye concentration inside the fibre was essentially zero.

In the presence of dye, an intrinsic signal would combine additively with the dye-dependent signal:

$$\Delta A(\lambda,t) = \Delta A_d(\lambda,t) + \Delta A_i(\lambda,t), \quad (6)$$

where each term represents an absorbance change at wave-length λ and time t and A, A_d and A_i represent respectively the total, dye-dependent and intrinsic signals.

Let us assume that the dye-related term is of the following form:

$$\Delta A_d(\lambda,t) = C(t)\Delta\epsilon(\lambda)\, 0{\cdot}7p, \tag{7}$$

where $C(t)$ is the time course of concentration of the calcium–dye complex, $\Delta\epsilon(\lambda)$ its differential extinction coefficient (a function of wave-length only) and p the length of the light path inside the fibre. We may assume a similar form for the intrinsic signal,

$$\Delta A_i(\lambda,t) = \alpha(t)\, f(\lambda)\, p, \tag{8}$$

where $\alpha(t)$ gives the time course of the intrinsic signal and $f(\lambda)$ specifies its wave-length dependence. Since calcium causes no change in dye absorbance at 790 nm, $\Delta A_i(\lambda,t)$ must be proportional to ΔA (790, t).

TABLE 1. Linear combination of signals at three different wave-lengths

Fibre	[Dye] (μM)	a*	b*	$\Delta\epsilon_{720}/\Delta\epsilon_{550}$
B11	760	0·282	0·319	−0·884
B14	485	0·684	0·559	−1·224
B19	480	0·433	0·737	−0·588
	611	0·766	0·717	−1·068
B23	334	0·209	0·192	−1·089
	575	0·146	0·184	−0·791
B90	400	0·249	0·365	−0·682
	560	0·313	0·387	−0·809
	660	0·367	0·432	−0·867
	690	0·349	0·343	−1·017
	750	0·396	0·414	−0·956
B94	126	0·234	0·251	−0·931
	279	0·319	0·380	−0·840
Mean				−0·904
S.D.				0·172

* Values of the coefficients a and b that give the least-squares value of $z = a\Delta A_{550} + b\Delta A_{720} + \Delta A_{790}$.

Eqns. (6–8) imply that the records at 550, 720 and 790 nm constitute a linearly dependent set, i.e. if the equations are correct it should be possible to find a zero linear combination $z(t)$ of the three records such that

$$z(t) = a\Delta A(550, t) + b\Delta A(720, t) + \Delta A(790, t) = 0. \tag{9}$$

The record $z(t)$ is represented in Fig. 9*D*. The coefficients a and b were found by minimizing the mean square value of z. The same procedure was applied to thirteen sets of records from six fibres. It was always possible to find a linear combination $z(t)$ not significantly different from the base line noise.

The existence of two components in the signal precludes direct evaluation of the differential extinction coefficients of the dye signal in the fibre, which should be compared to the values obtained in solution. However, the procedure of forming a vanishing linear combination provides a convenient alternative approach. Combining eqns. (6)–(9), it can be demonstrated that $a/b = -\Delta\epsilon(720)/\Delta\epsilon(550)$. The values of a, b and their ratio for the six fibres are listed in Table 1. The average value −0·904

of this ratio is remarkably close to 0·900, the value obtained by Rios & Schneider (1981*a*) in calibration solutions. This indicates that the dye-dependent component of the signal recorded at 720 or 550 nm is indeed due to the formation of a calcium–dye complex, which should be the same complex that dominates the reaction in solution, i.e. CaD_2. These observations confirm those of Baylor *et al.* (1982*a*), who used a wider range of wave-lengths and found that the early change in AP III absorbance after an action potential in intact dye-injected fibres closely followed the calcium difference spectrum of AP III in solution. They are not consistent with those of Palade & Vergara (1982, Fig. 8), which show a much smaller AP III-related absorbance change at 550 nm than at 710 nm.

The consideration given here to the intrinsic component of the signal should not convey the impression that it constituted a major interference. It was negligible in adequately stretched fibres and at dye concentrations greater than 200–300 μM and was generally smaller near 700 nm than near 500 nm.

In the remainder of this paper we will be considering only absorbance changes recorded at 700 or 720 nm. These will be denoted simply as ΔA, without indication of wave-length. In general, these signals were recorded at relatively high dye concentrations so that correction for intrinsic absorbance changes was unnecessary.

Calculation of free calcium transients from absorbance records

Fig. 10*A* presents a family of ΔA records for 100 msec pulses to the seven different membrane potentials marked next to the corresponding records in Part B. The pulse timing is indicated below the records. The ΔA records exhibit the pulse voltage-dependent characteristics of decreasing latency, increasing rate of rise, increasing peak value and increasing apparent steady level with increasing depolarization (Kovacs *et al.* 1979).

If only one calcium–dye complex were formed, each value of ΔA would be directly proportional to the concentration of the complex present in the fibre. In solution calibrations of the calcium : AP III reaction, the predominant product has been shown to be CaD_2 (Rios & Schneider, 1981*a* and present paper) for calcium and dye concentration ranges similar to those encountered in the present muscle fibre experiments. Moreover, it was shown in a previous section that, at the wave-lengths used in these experiments,the spectral properties of the signal are the same as those of CaD_2 in calibrations. Assuming the reaction to be the same inside muscle fibres, ΔA would be

$$\Delta A = [CaD_2]\,\Delta\epsilon\,0{\cdot}7p, \tag{10}$$

where $\Delta\epsilon$ is the change in dye extinction coefficient, here at 700 or 720 nm depending on the wave-length of incident light, per unit change in CaD_2 concentration. The proportional relationship between ΔA and $[CaD_2]$ allows direct conversion between the two parameters, as shown by the two ordinate scales in Fig. 10*A*.

Assuming essentially instantaneous equilibration of the calcium : dye reaction (Scarpa, 1979; Rios & Schneider, 1981*a*), the time course of free calcium for each pulse in Fig. 10 can be calculated from the corresponding $[CaD_2]$ record using the equation for chemical equilibrium. For the calcium : dye stoichiometry of 1 : 2,

$$[Ca] = K_D[CaD_2]/[D]^2, \tag{11}$$

where [Ca] and [D] are the concentrations of free calcium and free dye, $[CaD_2]$ is the concentration of calcium–dye complex and K_D is the dissociation constant for the reaction. The total dye concentration $[D]_T$ is given by

$$[D]_T = [D] + 2[CaD_2], \tag{12}$$

so that eqn. (11) can be expressed as

$$[Ca] = K_D[CaD_2]/([D]_T - 2[CaD_2])^2. \tag{13}$$

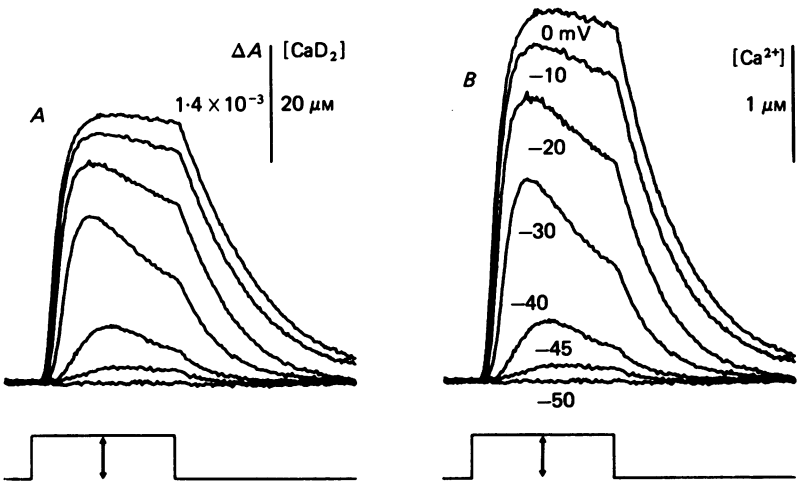

Fig. 10. Conversion of absorbance records to free calcium transients. *A*, absorbance changes at 720 nm elicited by 100 msec depolarizations to a variety of different membrane potentials. The vertical bar calibrates both the absorbance change (left scale) and the corresponding increase in concentration of the calcium–dye complex (right scale). *B*, time course of free Ca^{2+} concentration change calculated from the absorbance records in *A*. The vertical unit is equal to the unit of CaD_2 concentration in *A* multiplied by $K_D/[D]_T^2$, which equals the ratio of free to dye-bound calcium in the limit of low fractional reaction of dye. Each record in *A* and *B* is an average of two sweeps. The pulse timing is indicated below each family of records. Fibre B27, sequence 2. $s = 3{\cdot}49\ \mu m$, $d = 50\ \mu m$, $[D]_T = 590\ \mu M$.

Part *B* of Fig. 10 presents the [Ca] records calculated from the $[CaD_2]$ records of Part *A* using eqn. (13). The sets of [Ca] and $[CaD_2]$ records are generally similar in relative size and shape. The general voltage-dependent characteristics described above for the ΔA signals thus also apply to the calculated free calcium transients.

For $[CaD_2] \ll [D]_T$, eqn. (13) can be approximated by

$$[Ca] \simeq K_D[CaD_2]/[D]_T^2. \tag{14}$$

Thus, if the fraction of dye reacted with calcium were negligible, the free calcium concentration would be proportional to the concentration of calcium–dye complex CaD_2. In order to graphically represent the goodness of this approximation, the [Ca] records in Fig. 10*B* have been displayed so that a unit of Ca concentration is equal to $[D]_T^2/K_D$ times a unit of CaD_2 concentration in Part *A*. With these relative scales, the displayed sizes of the [Ca] and $[CaD_2]$ records would be identical if the fraction of dye reacted were negligible (eqn. 14). For the smallest pulses in Fig. 10 the [Ca] and $[CaD_2]$ records are approximately the same, indicating that the low fractional reaction approximation is applicable for these pulses. For the larger pulses that produced more calcium release, the displayed [Ca] records are somewhat expanded relative to their corresponding $[CaD_2]$

records, indicating that the fraction of dye reacted with calcium had become significant. Since the fractional reaction of dye was not negligible for some pulses, all [Ca] records were obtained using the complete equation (eqn. 13).

Effect of dye concentration on absorbance changes and calcium transients

During the course of each experiment the dye concentration in the central fibre segment increased continuously with time due to uninterrupted diffusion of dye into the fibre from its two cut ends. Except during fibre deterioration near the end of

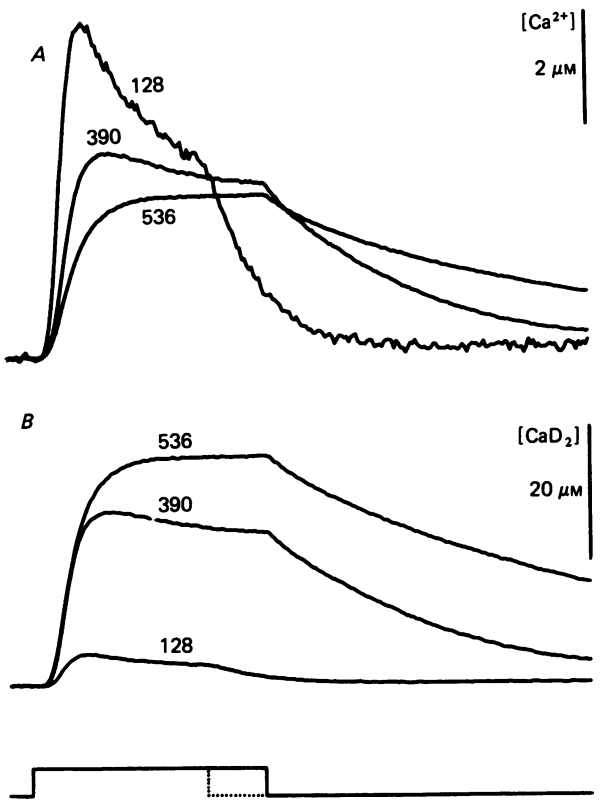

Fig. 11. Calcium transients for pulses to the same potential at various dye concentrations. *A*, changes in free calcium concentration at the three different dye concentrations indicated by the numbers next to each record (μM). *B*, changes in the concentration of calcium–dye complex corresponding to the [Ca] records in *A*. Pulses to −35 mV; duration of the pulses: 150 msec at the lowest dye concentration, 200 msec otherwise. Fibre B67. $s = 3{\cdot}78$ μm, $p = 60$ μm.

each experiment, the continuous increase in dye concentration was always accompanied by a continuous increase in the ΔA signal produced by a given pulse. This is illustrated in Part *B* of Fig. 11, which presents ΔA records, converted here to the proportional $[CaD_2]$ scale (eqn. 10), for pulses to −35 mV applied at three different times during dye entry. The pulse duration was initially 150 msec and was increased to 200 msec during the latter part of the experiment. The dye concentration present in the central fibre segment is indicated next to each record.

Part *A* of Fig. 11 presents the [Ca] transients corresponding to the [CaD_2] records in Part *B*. The [Ca] transients clearly were modified by the rising dye concentration. During the pulse the peak of the [Ca] transient was markedly depressed whereas the steady level that [Ca] appeared to be approaching was only slightly decreased. At the highest dye concentrations the peak in the [Ca] signal was completely suppressed and [Ca] increased monotonically toward its final level during the pulse. Following the pulse the return of [Ca] to its resting level was markedly slowed with increasing dye concentration. For each record in Fig. 11 *A* the decay of [Ca] after the pulse was well described by a single exponential function of time, with time constants ranging from 40 msec at 128 μM dye to 200 msec at 536 μM dye.

In experiments such as that in Fig. 11 the records at relatively high dye concentrations were obtained relatively late in the experiment. In order to verify that the observed effects were due to increasing dye concentration rather than simply to fibre run down, a few experiments were carried out with dye-containing solution applied only to one cut end and using longer central pools. By positioning the light slit at different points along the fibre, records were obtained at different dye concentrations at about the same time during the course of the experiment. The resulting [Ca] records exhibited effects of dye concentration similar to those in Fig. 11. Thus, fibre deterioration does not appear to be the source of the change in [Ca] records with changing dye concentration.

At any given dye concentration the shapes of the [CaS_2] and [Ca] signals in Fig. 11 are quite similar, indicating that the condition of relatively low fractional reaction of dye with calcium was roughly fulfilled. The maximum deviation of [Ca] from $K_D[CaD_2]/[D]_T^2$, its approximate relationship to [CaD_2] (eqn. 14), was 25% at the peak of the signal at 536 μM dye.

Comparing the families of [CaD_2] and [Ca] records in Figs. 11 *A* and *B*, it is apparent that there was a marked increase in the final level of [CaD_2] at high dye concentrations (Part *B*) even though the final level of [Ca] during the pulses decreased only slightly (Part *A*). In contrast, during the early part of the pulse the magnitudes of the [CaD_2] and [Ca] changes varied oppositely with increasing dye. Thus the calcium bound to dye at the end of these pulses at high dye concentrations was not obtained at the expense of a lowered free calcium. It must rather have been obtained from calcium that either would have been bound to myoplasmic calcium binding sites or would have been returned to the sarcoplasmic reticulum in the absence of dye. In contrast, relatively more of the calcium bound to dye early during the pulses was obtained from calcium that would have been free in the absence of dye. Close examination of the effect of dye concentration, as described in the next section, provides information for a quantitative estimation of the source of dye-bound calcium early during a pulse.

AP III increases the apparent myoplasmic volume for calcium

The concept of an increase in the apparent myoplasmic volume for calcium due to the presence of dye provides a convenient basis for interpreting the effects of dye concentration on the [Ca] transients. The concept arises directly from the approximately proportional relationship between dye-bound and free calcium. Assuming the calcium–dye reaction to be rapid compared to the [Ca] transient, calcium and dye would always be at equilibrium. For the calcium:dye stoichiometry of 1:2,

$[CaD_2]/[Ca]$ would then always equal $[D]^2/K_D$ (eqn. 11). Thus, for every unit of free calcium concentration in the myoplasm there would be $[D]^2/K_D$ times that unit of dye-reacted calcium. The net effect of having dye-reacted calcium is the same as would have been produced if the total free plus dye-reacted calcium had been dissolved in a volume of $1+[D]^2/K_D$ times the aqueous volume of the myoplasm. Following these considerations, the term $[D]^2/K_D$ can be thought of as an effective relative 'volume expansion' due to dye. For conditions of relatively low fractional reaction of dye with calcium, the volume expansion becomes a constant equal to $[D]_T^2/K_D$ (eqn. 14). For conditions where the reaction of dye with calcium is not negligible, the volume expansion is not constant but decreases with increasing [Ca].

The slowing of the decline of [Ca] following a given pulse with increasing dye concentration provides a straightforward example of the application of the volume expansion concept. Following each pulse the calcium release process can be assumed to be halted so that only processes involved in removing free calcium from the myoplasm need be considered. In many instances, including Fig. 11, the decline of [Ca] following a pulse has been experimentally observed to closely follow a single exponential time course (Kovacs *et al.* 1979). In such cases all calcium removal processes can be combined and treated as a single first-order uptake system for calcium. Such a system would remove calcium according to

$$dCa/dt = -\alpha[Ca], \tag{15}$$

where $-dCa/dt$ is the rate of removal of calcium from the myoplasm in units of amounts of calcium per unit time and α is a constant. To obtain the equation for the rate of decline of free calcium concentration, eqn. (15) must be divided by the myoplasmic volume V giving

$$d[Ca]/dt = -(\alpha/V)[(Ca]. \tag{16}$$

Thus the time constant V/α for the first-order decline of [Ca] is directly proportional to the myoplasmic volume.

We now return to the volume expansion concept and note that the V in eqn. (16) must be the total effective myoplasmic volume, corresponding to the true aqueous myoplasmic volume plus all effective extra volumes contributed by rapidly equilibrating calcium buffers. Thus,

$$V = V_A(1+[D]^2/K_D+E_I), \tag{17}$$

where V_A is the aqueous volume of the myoplasm, $[D]^2/K_D$ is the volume expansion due to dye and E_I is the analogous volume expansion due to all intrinsic calcium binding reactions that are in rapid equilibrium with myoplasmic [Ca]. If the fractional occupancy of the rapidly equilibrating intrinsic calcium binding sites were small, E_I would be approximately constant. Since the time constant τ for the decay of [Ca] following a pulse is proportional to V, eqn. (17) would then predict that τ should be a linear function of $[D]^2/K_D$. Fig. 12 presents a test of this prediction. The data are values of time constants obtained from single exponential fits to the decay of [Ca] after the pulse in the records in Fig. 11*A* and other similar records for 150 (open symbols) or 200 msec (filled symbols) pulses to the same potential in the same fibre. As predicted, the time constants increased linearly with $[D]^2/K_D$. This result

provides experimental support for the assumptions underlying eqn. (17), namely, rapid equilibration and 1:2 stoichiometry for the calcium:dye reaction in the fibre.

The intercept of the straight line in Fig. 12 with the ordinate axis gives the value of τ that would have applied to the decay of [Ca] following these relatively long pulses in the absence of dye. Its value was 37 msec for the fibre and pulses in Fig. 12.

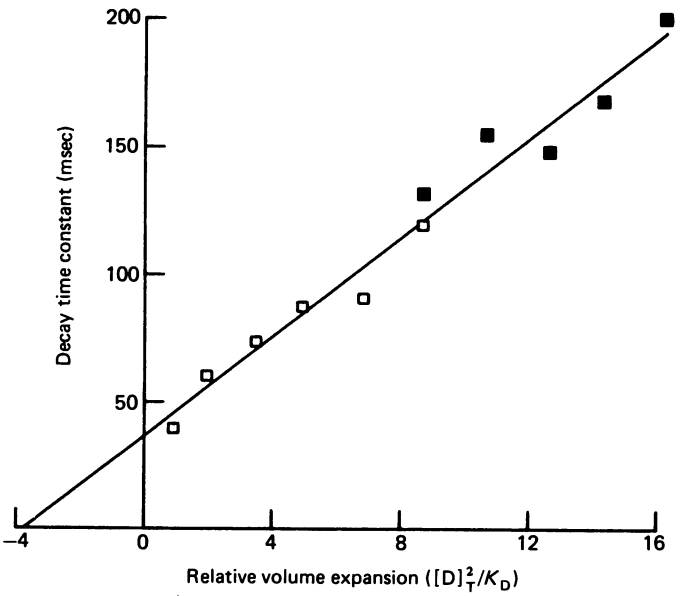

Fig. 12. Decay time constants as a function of 'volume expansion'. Ordinate: time constant obtained from single exponential fits to the decay after the pulse of the [Ca] records in Fig. 11 *A* and other similar records obtained for the same pulse in the same fibre at different dye concentrations. The depolarizing pulse was to −35 mV, its duration 150 msec at dye concentrations below 390 μm (□) and 200 msec otherwise (■). Abscissa: relative volume expansion due to the presence of dye, calculated as $[D]_T^2/K_D$ with $K_D = 17500\ \mu M^2$. Continuous line: linear regression, with ordinate intercept of 37·0 msec and slope 9·71 msec. Same fibre as in Fig. 11.

Intrinsic rapidly equilibrating calcium binding sites increase the apparent myoplasmic volume for calcium

The intercept of the line in Fig. 12 with the abcissa can be interpreted as the value of a hypothetical negative volume expansion that would have brought the total effective fibre volume to zero. Setting V equal to zero in eqn. (17) and defining Z as the negative value of $[D]^2$ at which the line in Fig. 12 crosses the abscissa, the expression

$$Z/K_D = -(1+E_I) \tag{18}$$

is obtained for the value of the intercept. Thus, in the absence of intrinsic rapidly equilibrating calcium binding reactions this intercept should be −1. Its value in Fig. 12 was −3·8, indicating a volume expansion of 2·8 times the myoplasmic aqueous volume contributed by rapid intrinsic calcium reactions after these relatively long pulses.

The estimate of intrinsic volume expansion depends critically on the value used

for K_D in Fig. 12. If K_D in the fibre differed from the value determined in calibrating solutions and used for Fig. 12, the abscissa scale in Fig. 12 would be in error. As an extreme example, if K_D in the fibre were actually 3·8 times higher than the value in solution, the value of $-(1+E_I)$ in Fig. 12 would be -1 and E_I would be 0. Any smaller value of K_D would be equally reasonable physically since it would give a value of $1+E_I$ greater than 1 and a positive E_I. Thus, from present results it is impossible to distinguish the effects of rapidly equilibrating intrinsic calcium-binding reactions from an improper value of K_D.

It is possible to utilize results such as those in Fig. 12 to provide a calibration that is independent of the value used for K_D. This is accomplished by monitoring the total concentration [Ca]* of free calcium plus calcium bound to rapidly equilibrating intrinsic buffers, which is given by

$$[Ca]^* = [Ca]\,(1+E_I). \tag{19}$$

Since the level of [Ca] calculated for any absorbance change is directly proportional to the value used for K_D (eqn. 11 or 13) whereas our estimate of $(1+E_I)$ is inversely proportional to the value of K_D (above discussion of Fig. 12), [Ca]* must be independent of K_D. Using a combined measure of free plus rapidly equilibrating intrinsically bound calcium thus avoids the K_D dependence involved in separating these two components.

In practice, monitoring [Ca]* rather than [Ca] simply involves a scale change and is conveniently implemented by changing the value of the dissociation constant used in converting from dye-bound to free calcium (eqn. 11). The value of this dissociation constant that would compute the [Ca]* defined in eqn. (19) as free calcium would be

$$K_D^* = K_D(1+E_I). \tag{20}$$

From (20) and (19)

$$K_D^*/K_D = [Ca]^*/[Ca]. \tag{21}$$

Multiplying (21) and (11),

$$[Ca]^* = K_D^*\,[CaD_2]/[D]^2, \tag{22}$$

that is, the calcium concentration calculated using K_D^* for K_D in eqn. (11) or (13) will be equal to [Ca]*. Combining eqns. (18) and (20) shows that K_D^* is equal to $-Z$. The abscissa intercept of the linear regression line fitted to the data in Fig. 12 gives a value of 66,700 μM^2 for K_D^*, or a [Ca]*/[Ca] of 3·8 (see above).

Monitoring the combined concentration of free plus rapidly equilibrating intrinsically bound calcium is convenient in analysing the effects of dye concentration at times early during calcium release. At such times calcium uptake and relatively slow calcium binding may be expected to be minimal so that dye-bound calcium should come predominantly from calcium that would otherwise be either free or bound to rapidly equilibrating intrinsic binding sites.

Effects of dye concentration during the early phases of calcium release

Fig. 13 presents an analysis of the effects of dye concentration early during the release process. Part *A* presents $[CaD_2]$ transients for a 30 msec pulse to -30 mV applied at various times during dye entry. The dye concentration present in the central fibre segment is indicated next to each record. The $[CaD_2]$ transients exhibit the previously mentioned increase in signal with increasing dye concentration.

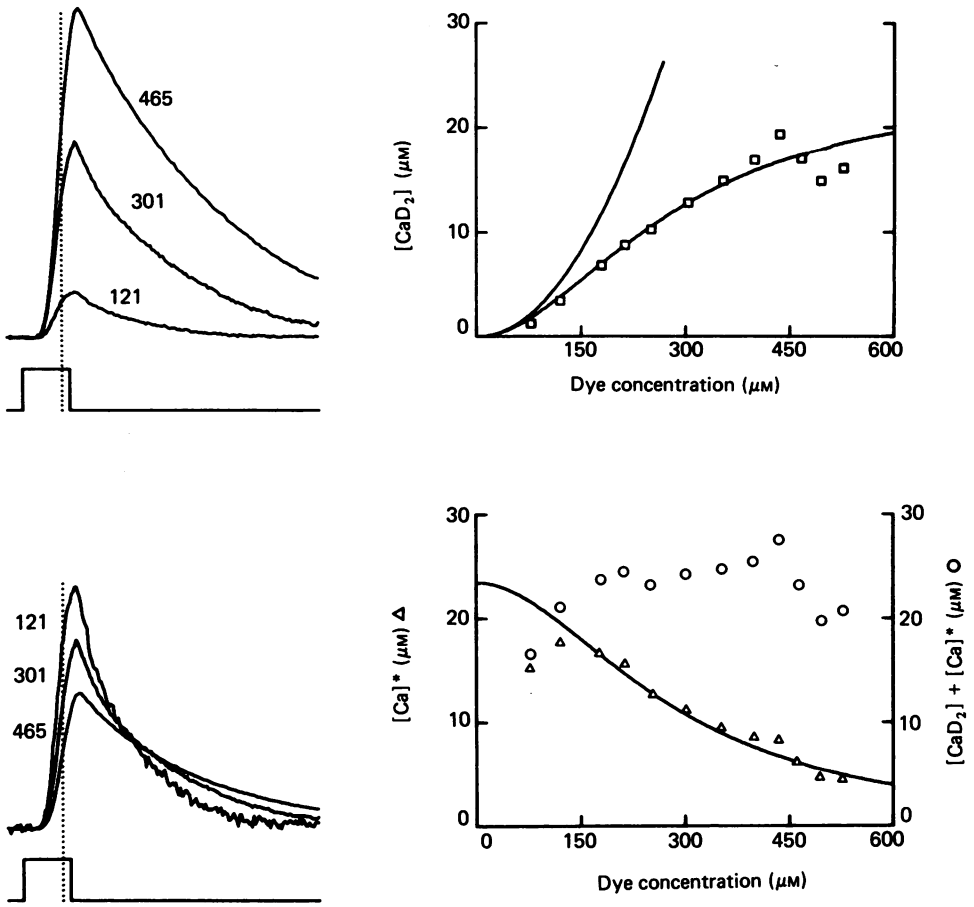

Fig. 13. Transient changes of calcium–dye complex and of free plus rapidly equilibrating calcium as a function of dye concentration. *A*, sample [CaD_2] transients due to depolarization of the fibre to −10 mV during 30 msec (voltage pulse represented schematically). Vertical scale: same as ordinate axis of Part *B*. The numbers next to each curve indicate the dye concentration (in μM) at the time the records were taken. Each record is an average of two sweeps; eleven such records were obtained for the same pulse during the experiment. The vertical dotted line indicates 25 msec after the beginning of the pulse. *B*, concentration of calcium–dye complex at 25 ms after the beginning of 30 msec pulses to −10 mV. The ordinate of the points in *B* corresponds to the intersection of the dotted line and the records in *A*. The curve through the points gives the theoretical relationship between concentration of calcium–dye complex and dye concentration assuming constant release of calcium, 1:2 calcium:dye stoichiometry and negligible uptake or slow binding (see text). The parabola is the limiting form of the theoretical relationship, at low dye concentrations. *C*, transient changes in free plus rapidly equilibrating intrinsically bound calcium [Ca]* calculated from the records in Part *A*. Vertical scale: same as left ordinate axis of Part *D*. *D*, (△) value of [Ca]* at 25 msec after the beginning of the pulse for the records in *C* as well as the other records included in Part *B*. (○) sum of [CaD_2] (from Part *B*) plus [Ca]*; these points correspond to the right ordinate axis. Same fibre as in Figs. 11 and 12.

Part *B* of Fig. 13 gives a graphical representation of the relationship between $[CaD_2]$ and dye concentration. The squares are values of $[CaD_2]$ at 25 msec after the start of each pulse, plotted as a function of the total dye concentration present in the central fibre segment at the time of pulse application. The 25 msec time was selected arbitrarily and is marked by the dashed vertical line in Part *A* of Fig. 13. The values for Part *B* were obtained from the records in Part *A* and from other records for the same pulse in the same experiment but not shown in Part *A*.

Using the procedure for calculating free plus rapidly equilibrating intrinsically bound calcium concentration from $[CaD_2]$ (eqn. (13) with $K_D = K_D^*$), the records in Fig. 13*A* can be re-examined to determine the effect of dye concentration on the [Ca]* transients. Part *C* of Fig. 13 presents a set of [Ca]* records calculated from the $[CaD_2]$ records in Part *A*. The dye concentration at the time of each pulse is indicated next to each [Ca]* record. As dye increased, the [Ca]* transient produced during the constant pulse decreased. Thus, at least some of the increase in calcium bound to dye with increasing dye concentration during these relatively short pulses (Part *A*) was obtained at the expense of [Ca]*. Such depression of [Ca]* by dye is to be expected from the effective volume expansion due to the calcium buffering action of the dye (above). It is interesting to note that the calcium buffering not only lowered [Ca]* during calcium release, but also slowed uptake so that at relatively long times after the pulse [Ca]* actually increased with increasing dye concentration.

Values of [Ca]* at 25 msec after the start of the pulse are presented graphically as a function of dye concentration in Part *D* of Fig. 13 (triangles). Comparison of Parts *B* and *D* of Fig. 13 reveals a roughly reciprocal increase of $[CaD_2]$ and decrease of [Ca]* with increasing total dye concentration. The data in Fig. 13 were obtained by applying the same pulse at various times during dye entry. For a stable fibre this should correspond to release of a set amount of calcium from the sarcoplasmic reticulum for each pulse, but into a myofilament space containing a varying dye concentration. At times early during calcium release both calcium uptake and slowly equilibrating calcium binding should be minimal. Under such conditions the sum of $[CaD_2]$ plus [Ca]* would be independent of $[D]_T$. Values of this sum at 25 msec after the start of the pulse are represented as circles in Part *D* of Fig. 13 and are roughly constant. Thus, uptake and slow binding probably accounted for relatively little of the released calcium at this early time during the release process.

Fig. 14 presents a further check for the reciprocal variation of $[CaD_2]$ and [Ca]* but constancy of $[CaD_2]+[Ca]^*$ with changing dye concentration, again using values obtained early during the release process. Part *A* of Fig. 14 presents values obtained at 25 msec after the start of pulses to -35 mV and Part *B* presents values for 12 msec into pulses to -10 mV, in each case for the same fibre as in Fig. 13. For both pulses there was a clearly reciprocal decrease of [Ca]* (triangles) and increase of $[CaD_2]$ (squares) as the dye concentration increased. The circles in each Part of Fig. 14 present the sum of [Ca]* and $[CaD_2]$. For each set of pulses $[Ca]^*+[CaD_2]$ was roughly constant with changing dye concentration, consistent with the assumption of constant release and minimal amounts of uptake or relatively slow binding of calcium at these early times during calcium release. The points at the three highest dye concentrations in Figs. 13 and 14 gave systematically low values of $[Ca]^*+[CaD_2]$, probably indicative of the beginning of fibre run down.

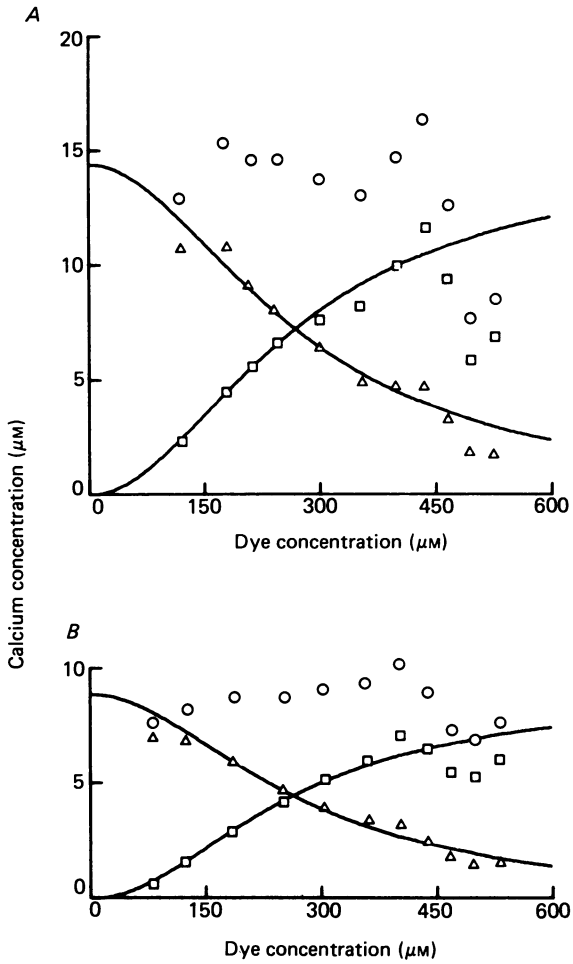

Fig. 14. Forms of released calcium early during the release process as a function of dye concentration. *A*, values of $[CaD_2]$ (□), $[Ca]^*$ (△) and $[CaD_2]+[Ca]^*$ (○) at 25 msec after the start of pulses to −35 mV repeated at various dye concentrations as represented in the abscissa. The curve through the squares is a plot of the theoretical dependence of $[CaD_2]$ on dye concentration for the 1:2 stoichiometry (eqn. 33). The parameter values used for the theoretical curve were $K_D^* = 66{,}700\ \mu M^2$, an independent estimate obtained from an analysis of the decay time constants after relatively long pulses in the same fibre (Fig. 12) as explained in the text, and the total calcium release $R = 14{\cdot}38\ \mu M$, an average of all vaues of $[CaD_2]+[Ca]^*$ excluding the last three. The curve through the triangles is the difference between R and the first curve. *B*, same as Part *A* but at 12 msec into a pulse to −10 V. For the theoretical curves in Part *B*, $K_D^* = 66{,}700\ \mu M^2$ and $R = 8{\cdot}87\ \mu M$, the average of all but the last three circles. Same fibre as in Figs. 11–13.

Further evidence for a calcium:dye stoichiometry of 1:2 in the myoplasm

The observed relationships between concentration of calcium–dye complex and total dye concentration presented as squares in Figs. 13 and 14 provide another source of information regarding the calcium:dye stoichiometry in the fibre. The fact that these data follow a relationship that is concave up near the origin is a direct

qualitative indication that the calcium–dye reation in the fibre must be higher than first order in dye.

Although plotted as values of $[CaD_2]$, the squares in Figs. 13*B* and 14 were determined from absorbance changes and are thus simply proportional to the concentration $[Ca_nD_m]$ of calcium–dye complex for any calcium:dye stoichiometry n:m (e.g. eqn. (10) for the 1:2 stoichiometry). The observed dependence of $[Ca_nD_m]$ on dye concentration can be compared quantitatively with the theoretical predictions for various stoichiometries. In carrying out such comparisons, we shall neglect both calcium uptake and slowly equilibrating calcium binding at early times during a pulse (previous section); we shall assume constant calcium release and essentially instantaneous equilibration of calcium and dye. Under such conditions the data can be interpreted using the equations for chemical equilibrium with the sum of $n[Ca_nD_m]$ plus [Ca]* constant and equal to the free calcium concentration that the set amount of released calcium would give if all dissolved in the myoplasmic volume. The theoretical relationships between $[Ca_nD_m]$ and $[D]_T$ predicted for these conditions for the calcium:dye stoichiometries of 1:1 and 1:2 are derived in the Appendix.

The observed relationships between $[Ca_nD_m]$ and $[D]_T$ are consistent with the predictions for the 1:2 stoichiometry with constant total calcium. At low $[D]_T$ this stoichiometry predicts a quadratic relationship between $[CaD_2]$ and $[D]_T$ that passes through the origin with zero slope (Appendix), and is represented by the parabola in Fig. 13 *B* (upper curve). At higher dye concentrations calcium becomes limiting and the predicted relationship bends away below the parabola as shown by the lower curve in Fig. 13 *B*. At very high dye levels almost all released calcium would react with dye so that the lower curve would eventually approach a constant asymptote equal to the value of $[CaD_2]$ for complete reaction of all released calcium with dye. The data in Figs. 13 *B* and 14, as well as those for other pulses and other fibres, qualitatively followed this type of relationship.

The observed relationships between $[Ca_nD_m]$ and $[D]_T$ given by the squares in Figs. 13*B* and 14 are inconsistent with the predictions for the 1:1 stoichiometry. For relatively low levels of $[D]_T$ the 1:1 stoichiometry predicts a linear relationship between [CaD] and $[D]_T$ that passes through the origin with positive slope (Appendix). With increasing $[D]_T$ the relationship decreases in slope, bending away below the extrapolated low dye straight line. At high $[D]_T$ the theoretical relationship for 1:1 stoichiometry also approaches a constant asymptote, here equal to the value of [CaD] for reaction of all released calcium with dye. For the 1:1 stoichiometry the maximum slope of the [CaD] *vs.* $[D]_T$ plot is thus obtained at the origin. Straight lines forced to fit the theoretical relationship for the 1:1 stoichiometry at higher $[D]_T$ ranges would have smaller slopes and would tend to intersect the ordinate axis at positive values of [CaD]. These predictions for the 1:1 stoichiometry are clearly in contrast to the observations in Figs. 13*B* and 14. The $[Ca_nD_m]$ values (squares) follow a relationship that first increases in slope with increasing $[D]_T$ at low dye concentrations and then decreases in slope at higher dye. Straight lines forced to fit to the $[Ca_nD_m]$ data over the lower dye concentration ranges in Figs. 13*B* and 14 would extrapolate to intersect the ordinate axis at negative values of $[Ca_nD_m]$, not at zero or positive values as predicted for the 1:1 stoichiometry relationship.

All values of [Ca]* and all the theoretical curves in Figs. 13 and 14 were calculated using the value 67,500 μM^2 for K_D^*, an independent estimate obtained from the effect of $[D]_T$ on the time constant for [Ca] decay after long pulses in the same fibre (Fig. 12). The data of Fig. 14*B*, which were obtained using the relatively large pulse to −10 mV, were measured at 12 msec after the start of the pulse. Data at later times

into these pulses could not be fit by the theoretical relationship unless we used a larger value for K_D^*. This is to be expected as the theoretical calculation assumes negligible removal of calcium by uptake and relatively slow binding processes. This assumption probably does not hold at times later than 12 ms into the pulses to −10 mV. At these times a significant amount of calcium may have been removed by those processes. To account for such removed calcium in our calculations, it could be roughly assigned to the rapidly equilibrating intrinsic buffers by increasing the estimates of K_D^* and E_I.

DISCUSSION

AP III as a minimally perturbing indicator for calcium transients

The results presented in this paper demonstrate that the metallochromic indicator dye antipyrylazo III can be used to monitor myoplasmic calcium transients in muscle fibres with no obvious deleterious effects on the fibre. However, the presence of the dye at relatively high concentrations itself caused major modifications of the amplitude and time course of the calcium transient. The question thus arises as to whether this dye is practical for use as a *non-perturbing* indicator of the calcium transient. A qualitative answer can be obtained from examination of sets of calcium transients recorded for the same pulse at different dye concentrations, such as the records for relatively long pulses in Fig. 11*A*. From these and other records for the same pulse in the same fibre, one obtains the impression that the calcium transient that would have occurred in the absence of dye would have been slightly more peaked and slightly more rapidly decaying both during and after the pulse than was the case for the transient recorded at the lowest dye concentration of 128 μM. A more quantitative answer can be given. To the extent that the assumptions of constant release with varying dye concentration and of negligible uptake early during the release process are valid, the theoretical curves in Fig. 14 indicate that at 25 msec into the pulse to −35 mV (Part *A*) and at 12 msec into the pulse to −10 mV (Part *B*), the calcium transients at 125 μM dye were respectively only 15 and 17 % less than they would have been in the dye-free fibre. The theoretical line in Fig. 12 indicates that the decay time constant after relatively long pulses to −35 mV was only 6 % longer at 125 μM-dye than it would have been in the dye-free fibre. Thus, the calcium transients recorded at or below 125 μM were minimally distorted by the dye. At 125 μM-dye they also had clearly acceptable signal to noise ratios, as can be seen in Figs. 11*A* and 13*C*. Thus, at these concentrations the dye acts as a practical minimally-perturbing indicator for myoplasmic calcium.

It must be noted, however, that all values of [Ca] obtained with AP III, including those obtained at low dye concentrations, are directly proportional to the value used for K_D. Their accuracy is thus only as good as the agreement of the K_D of AP III in the fibre with its value in caesium glutamate calibration solution at 5 °C. Clearly, a direct calibration of the dye inside the fibre, such as has been carried out for arsenazo in squid giant axons (Dipolo, Requena, Brinley, Mullins, Scarpa & Tiffert, 1976), would be desirable. Unfortunately, in our muscle fibre preparation we rely on the relatively slow process of diffusion to alter the internal medium rather than the more rapid perfusion or dialysis techniques possible with giant axons so that such direct calibration has thus far not been achieved inside muscle fibres.

AP III as a modifier of calcium transients: analysis of effects of dye concentration

At higher concentrations, AP III caused major modifications of the calcium transient. Quantitative study of such modifications provided information regarding the stoichiometry of the calcium:dye reaction in the fibre. Analyses of the variation with dye concentration of (1) the concentration of calcium–dye complex at a given time early during a given pulse and (2) the decay time constant of the calcium transient after relatively long pulses provided two independent sets of data, both of which indicated that the calcium:AP III stoichiometry was 1:2 in the fibre as was the case in calibrating solution. The agreement of the wave-length dependencies of the calcium–dye signal in the fibre and in calibrating solutions is further evidence of the similarity of dye properties under the two conditions.

The quantitative study of the modification of calcium transients by the dye also provided information about fibre properties. Analysis of the effect of dye concentration on the decay time constant after long pulses provided evidence for the presence of rapidly equilibrating calcium-binding reactions intrinsic to the fibre. The effect of dye concentration on decay time constants after shorter pulses was also indicative of the presence of such rapid intrinsic calcium-binding reactions (W. Melzer, E. Rios & M. F. Schneider, unpublished observations). Exact quantification of the amount of intrinsic rapidly equilibrating calcium buffer depends directly on the value used for the Ca–AP III dissociation constant K_D in the fibre. However, the decay time constant data do provide sufficient information to allow an exact quantification of the combined concentration [Ca]* of free calcium plus calcium bound to rapidly equilibrating intrinsic buffers, independent of K_D. This is accomplished through the use of the apparent dissociation constant K_D^* as described in the Results section.

The data on the effect of dye concentration on $[Ca]^* + [CaD_2]$ at a given time early during the release process (Figs. 13 and 14) provide an independent check of the [Ca]* calculation. Assuming release to be independent of dye concentration and calcium uptake and relative slow binding to be negligible early during release, $[Ca]^* + [CaD_2]$ should be independent of dye concentration. Within experimental error, this appeared to be the case for the pulses in Figs. 13 and 14. For those Figures [Ca]* was calculated using the value of K_D^* obtained independently from the analysis of the effect of dye concentration on the decay time constant after long pulses in the same fibre. An appreciably different value of K_D^* would not be compatible with constancy of $[Ca]^* + [CaD_2]$ early during these pulses. Thus, the data in Figs. 13 and 14 provide an independent check of the validity of the value of K_D^* obtained from the data in Fig. 12.

Use of the volume expansion concept to interpret the effects of dye concentration

In order to interpret the effects of dye concentration on the calcium transients, we developed the concept of the dye causing an apparent expansion of the myoplasmic volume. A simple simulation demonstrates that such volume expansion may be sufficient to account for all dye effects on the calcium transients. The simulation is based on the cyclic three-compartment system for intracellular calcium redistribution shown in Fig. 15 (Kovacs *et al.* 1979; Schneider *et al.* 1981), with the fractional transfer coefficients f_{ji} for transfer into compartment j from compartment i assumed to have

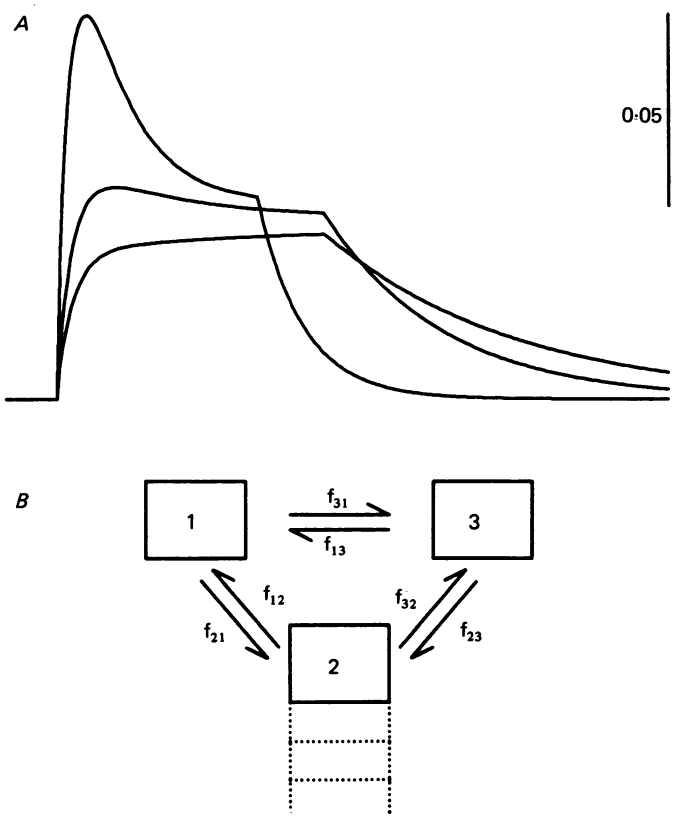

Fig. 15. Simulation of the effect of dye concentration on calcium transients using a cyclic three-compartment model for redistribution of intracellular calcium. *A*, computer generated time courses of concentrations in compartment 2 of the model in Part *B*. The top record was generated using the following constant values for the theoretical fractional transfer coefficients f_{ij} (sec^{-1}) during the pulse: $f_{21} = 140$, $f_{12} = 20$, $f_{32} = 60$, $f_{23} = 0$, $f_{31} = 22{\cdot}6$, $f_{13} = 4$. The initial fractional contents in compartments 1, 2 and 3 were 0·18, 0·015, 0·805, respectively. These values were selected arbitrarily in order to generate a record similar to the experimental record obtained at the lowest dye concentration (128 μM) in Fig. 11. The decline in calcium in compartment 2 after the pulse was generated assuming $f_{21} = f_{12} = 0$, with all other coefficients unchanged. The second and third records were generated by introducing in the model an expansion in the volume of compartment 2 consistent with the increased dye concentrations (390 and 536 μM). The ratios between expanded volumes and the reference volume were calculated as $(1 + D_1^2/K_D^*)/(1 + D_1^2/K_D^*)$, where D_1 was 128 μM and D_1 was either 390 or 536 μM. $K_D^* = 66{,}700$. Vertical scale: fraction of total calcium present in compartment 2. Duration of 'on' portions of the simulated records: 140 and 190 msec.

constant values either during or after a pulse. Such a model is clearly a crude first approximation since release does not turn on instantly at the start of a pulse (Kovacs *et al.* 1979) and the uptake rate constant changes depending on past history (Kovacs *et al.* 1979; W. Melzer, E. Rios & M. F. Schneider, unpublished observations). Nonetheless, the model does provide a simplified example that illustrates how the volume expansion due to dye could operate to modify the calcium transient in the observed manner.

Using the model, a set of values for the transfer coefficients and initial fractional contents of each compartment were somewhat arbitrarily selected so as to generate a calcium transient in compartment 2 that resembled the transient at the lowest dye concentration (128 μM) in Fig. 11 *A*. Records at different dye concentrations were then simulated by considering the change in the effective volume due to dye to be the only direct effect of a change in dye concentration. This was carried out by setting the ratio of the effective volumes at dye concentration $[D]_i$ to that at $[D]_1$ equal to $(1+[D]_i^2/K_D^*)/(1+[D]_1^2/K_D^*)$, where $[D]_1$ was 128 μM, $[D]_i$ was 390 or 536 μM and K_D^* was 66,700 μM^2, as determined from Fig. 12. For each of the higher concentrations, the transfer coefficients f_{12} and f_{32} for movement out of compartment 2 were simply reduced in inverse proportion to the ratio of effective volume of compartment 2, with all other coefficients assumed to be unchanged. The resulting records in Fig. 15 closely simulate those at the two higher dye concentrations in Fig. 11 *A*, indicating that volume expansion due to dye is sufficient to explain the observed effects of dye concentration on the calcium transients.

Concluding comments

At the outset, we mentioned that monitoring calcium transients is of interest for understanding both myofilament activation and sarcoplasmic reticulum calcium release. Within the uncertainties outlined above, the time course of [Ca] can now be monitored in our voltage clampled cut single muscle fibre preparation. Using such data together with published values for calcium binding and unbinding rate constants for troponin, it is possible to calculate the time course of calcium binding to troponin. This sort of calculation has been carried out in other laboratories (Robertson, Johnson & Potter, 1981; S. M. Baylor, W. K. Chandler & M. W. Marshall, personal communication). In order to use the recorded [Ca] transients to estimate calcium release, it is necessary to know the time courses of not only [Ca]* and $[CaD_2]$ but also those of calcium uptake and relatively slow calcium binding. The present paper establishes procedures for monitoring [Ca]* and $[CaD_2]$. Procedures for characterizing uptake and relatively slow binding and for using that information to calculate the time course of calcium release are currently being developed (Melzer, Rios & Schneider, 1983).

APPENDIX

Concentration of calcium–dye complex early during calcium release as a function of dye concentration

This appendix provides theoretical expressions for the change in concentration of calcium–dye complex due to release of a constant amount of calcium into the myofilament space as a function of the total dye concentration present in that space. The special conditions of negligible uptake and negligible slow binding of the released calcium are assumed to apply.

In order to simplify the notation for the derivations in this appendix, brackets have been eliminated and the following concentrations have been denoted by the indicated symbols: concentration [Ca] of free calcium, *F;* concentration of calcium bound to rapidly equilibrating intrinsic binding sites, *I;* concentrations $[D]_T$ and [D] of total and calcium-free dye, D_T and *D;* concentrations [CaD] or $[CaD_2]$ of calcium bound

to dye for the 1:1 or 1:2 calcium:dye stoichiometries, both denoted by B since for both these stoichiometries the concentration of calcium bound to dye is simply equal to the concentration of calcium–dye complex.

It is assumed that the amount of calcium released during a given short interval starting at the beginning of a given depolarizing pulse is a constant, independent of the dye concentration in the myoplasm. It is also assumed that this amount of released calcium, which would attain concentration R if all freely dissolved in the myoplasm, distributes among only three states or forms: free in solution, bound to rapidly equilibrating intrinsic buffers and bound to the dye. These three forms are assumed to be in equilibrium. As a final assumption, the rapid intrinsic calcium-binding reactions are considered to be far from saturation and of adequate stoichiometry so that I is equal to $F \cdot E_I$, where E_I is the relative volume expansion due to rapid intrinsic buffers as defined in the text. Under these assumptions,

$$R = F(1+E_I)+B. \tag{23}$$

The functional relationship between B and D_T depends critically on the stoichiometry assumed for the calcium:dye reaction. Two alternative candidate stoichiometries, 1:1 and 1:2, will be considered in these derivations.

If the stoichiometry of the calcium–dye reaction is 1:1, the following equations hold:

$$K_D = FD/B, \tag{24}$$

$$D = D_T - B. \tag{25}$$

Eqns. (24) and (25) can be substituted in (23) to obtain

$$B^2 - B(R+D_T+K_D^*)+RD_T = 0, \tag{26}$$

where

$$K_D^* = K_D(1+E_I). \tag{27}$$

The quadratic equation is of course the general equation relating equilibrium concentration of product (B) to total concentration of reactants (R and D_T) in a 1:1 reaction, the only effect of the intrinsic buffering being the introduction of the apparent dissociation constant K_D^* defined in eqn. (27) and discussed in the text.

The dependence of B on D_T can be obtained by solving eqn. (26) for B. In the limit of low D_T, both D_T and D will be $\ll R$ so that eqn. (26) reduces to

$$B = [R/(K_D^*+R)]D_T. \tag{28}$$

In the limit of very high D_T, eqn. (26) reduces to $B = R$. At intermediate D_T, the complete solution to eqn. (26) is needed.

If the stoichiometry of the calcium:dye reaction is 1:2, the equilibrium and material balance equations are different:

$$K_D = FD^2/B, \tag{29}$$

$$D = D_T - 2B. \tag{30}$$

From eqns. (23), (29) and (30) we obtain an equation analogous to (26), but cubic in B for the 1:2 stoichiometry:

$$B^3 - B^2(D_T+R)+B(K_D^*/4+RD_T+D_T^2/4)-RD_T^2/4 = 0. \tag{31}$$

This equation is solvable by standard procedures (Bronshtein & Semendiaev, 1973). It can be put in the form

$$y^3+3py+2q=0, \tag{32}$$

where the new parameters are defined as

$$\begin{aligned} y &= B+b/3,\\ 2q &= 2b^3/27-bc/3+d,\\ 3p &= c-b^2/3,\\ b &= -(D_T+R),\\ c &= K_D^*/4+rD_T+D_T^2/4,\\ d &= -RD_T^2/4. \end{aligned}$$

Eqn. (32) has explicit solutions, 'Cardano's formulas' (Bronshtein & Semendiaev, 1973); in the present case only the first root is real, and is given by

$$y_1=[(p^3+q^2)^{\frac{1}{2}}-q]^{\frac{1}{3}}+[-(p^3+q^2)^{\frac{1}{2}}-q]^{\frac{1}{3}}. \tag{33}$$

From eqn. (33) and the parameter definitions, B was obtained as a function of D_T and is represented as the sigmoid curve in Figs. 13*B*, 14*A* and *B*.

It is interesting to find a limiting form for eqn. (33) at low D_T as the differences in the functional relationship $B(D_T)$ for the two stoichiometries should be most striking at those values of D_T. From eqn. (29) and (23) we obtain

$$B(1+K_D^*/D^2)=R, \tag{34}$$

or

$$B=RD^2/(D^2+K_D^*), \tag{35}$$

which at low D_T simplifies to

$$B=RD^2/K_D^*. \tag{36}$$

Introducing eqn. (30) in eqn. (36) and rearranging, we obtain a quadratic equation that solves to

$$2B=D_T+A-(2D_TA+A^2)^{\frac{1}{2}}, \tag{37}$$

where A is the constant $K_D^*/4R$. From eqn. (37) it can be seen that

$$\lim_{D_T\to 0}\frac{dB}{dD_T}=0, \tag{38}$$

$$\lim_{D_T\to 0}\frac{d^2B}{dD_T^2}=\frac{2R}{K_D^*}, \tag{39}$$

or equivalently

$$B\simeq (R/K_D^*)D_T^2. \tag{40}$$

The limiting expression (40) was represented as a parabola in Fig. 13*B*.

We thank Dr Werner Melzer for stimulating suggestions and for helping with the dye calibration measurements, data analysis and figure preparation, Mr James Costantin for determining the absorption spectrum of antipyrylazo III in solution and for skilled general technical assistance, Mr John Young for maintaining our digital instrumentation and computers, Drs S. M. Baylor, W. K. Chandler and M .W. Marshall for providing preliminary versions of their papers (1982), Dr R. F. Rakowski for information regarding the diffusion of arsenazo III in muscle fibres and Mss Karen Vogt and Wendy Keck for their skilled typing and perseverance. This work was supported by research grants from the U.S.P.H.S. (RO1-NS13842) and the Muscular Dystrophy Association.

REFERENCES

BAYLOR, S. M., CHANDLER, W. K. & MARSHALL, M. W. (1982*a*). Optical measurements of intracellular pH and magnesium in frog skeletal muscle fibres. *J. Physiol.* **331**, 105–138.

BAYLOR, S. M., CHANDLER, W. K. & MARSHALL, M. W. (1982*b*). Use of metallochromic dyes to measure changes in myoplasmic calcium during activity in frog skeletal muscle fibres. *J. Physiol.* **331**, 139–178.

BEELER, T. J., SCHIBECHI, A. & MARTONOSI, A. (1980). The binding of Arsenazo III to cell components. *Biochim. biophys. Acta* **629**, 317–327.

BLINKS, J. R. (1978). Measurement of calcium ion concentrations with photoproteins. *Ann. N.Y. Acad. Sci.* **207**, 71–85.

BLINKS, J. R., WEIR, W. G., HESS, P. & PRENDERGAST, F. G. (1982). Measurement of Ca^{2+} concentration in living cells. *Prog. Biophys. molec. Biol.* **40**, 1–114.

BRONSHTEIN, I. & SEMENDIAEV, K. (1973). *Manual de Matematicas.* Moscow: MIR.

CARLSLAW, H. S. & JAEGER, J. C. (1947). *Conduction of Heat in Solids.* Oxford University Press.

CHANDLER, W. K., RAKOWSKI, R. F. & SCHNEIDER, M. F. (1976). A non-linear voltage dependent change movement in frog skeletal muscle. *J. Physiol.* **254**, 245–283.

CRANK, J. (1975). *The Mathematics of Diffusion.* Oxford: Clarendon Press.

DIPOLO, R., REQUENA, J., BRINLEY, F. J., MULLINS, L. J., SCARPA, A. & TIFFERT, T. (1976). Ionized calcium concentrations in squid axons. *J. gen. Physiol.* **67**, 433–467.

FABIATO, A. & FABIATO, F. (1975). Effects of magnesium on contractile activation of skinned cardiac cells. *J. Physiol.* **249**, 497–517.

HARAFUJI, H. & OGAWA, Y. (1980). Reexamination of the apparent binding constant of ethylene glycol bis (β-aminoethyl ether)-N,N,N′,N′-tetraacetic acid with calcium around neutral pH. *J. Biochem.* **87**, 1305–1312.

HOBBIE, R. K. (1978). *Intermediate Physics for Medicine and Biology.* New York: Wiley.

KOVACS, L., RIOS, E. & SCHNEIDER, M. F. (1979). Calcium transients and intramembrane charge movement in skeletal muscle fibres. *Nature, Lond.* **279**, 391–396.

KOVACS, L. & SCHNEIDER, M. F. (1977). An increase in optical transparency associated with excitation–contraction coupling in voltage-clamped cut skeletal muscle fibres. *Nature, Lond.* **265**, 556–560.

KOVACS, L. & SCHNEIDER, M. F. (1978). Contractile activation by voltage clamp depolarization of cut skeletal muscle fibres. *J. Physiol.* **277**, 483–506.

KOVACS, L. & SZUCS, G. (1980). Effect of caffeine on mechanical activation in cut skeletal muscle fibres. In *Adv. Physiol Sci.*, vol. 5. *Molecular and Cellular Aspects of Muscle Function*, ed. VARGA, E., KOVER, A., KOVACS, T. & KOVACS, L., pp. 341–344. London: Pergamon Press.

MARTELL, A. E. & SMITH, R. M. (1974). *Critical Stability Constants*, vol. 1. New York: Plenum Publishing Corp.

MELZER, W., RIOS, E. & SCHNEIDER, M. F. (1983). Rate of calcium release in frog skeletal muscle. *Biophys. J.* **41**, 396a.

MILEDI, R., PARKER, I. & SCHALOW, G. (1977). Measurement of calcium transients in frog muscle by the use of arsenazo III. *Proc. R. Soc.* B **198**, 201–210.

PALADE, P. & VERGARA, J. (1981). Detection of Ca^{++} with optical methods. In *The Regulation of Muscle Contraction: Excitation–Contraction Coupling*, ed. GRINNELL, A. D. & BRAZIER, M. A. B., pp. 143–158. New York: Academic Press, Inc.

PALADE, P. & VERGARA, J. (1982). Arsenazo III and antipyrylazo III calcium transients in single skeletal muscle fibers. *J. gen. Physiol.* **79**, 679–708.

RIOS, E. & SCHNEIDER, M. F. (1981*a*). Stoichiometry of the reactions of calcium with the metallochromic indicator dyes Antipyrylazo III and Arsenazo III. *Biophys. J.* **36**, 607–621.

RIOS, E. & SCHNEIDER, M. F. (1981*b*). Antipyrylazo III in skeletal muscle fibres: a calcium indicator and a calcium buffer. 7th International Biophysics Congress. Mexico City, p. 176.

RIOS, E. & SCHNEIDER, M. F. (1982). The time course of free myoplasmic calcium in skeletal muscle fibres as monitored and modified by the dye Antipyrylazo III. *Biophys. J.* **37**, 22a.

ROBERTSON, S. P., JOHNSON, J. D. & POTTER, J. D. (1981). The time-course of Ca^{++} exchange with calmodulin, troponin, parvabumin, and myosin in response to transient increases in Ca^{++}. *Biophys. J.* **34**, 559–569.

SCARPA, A. (1979). Measurement of calcium ion concentrations with metallochromic indicators. In *Detection and Measurement of Free Ca^{2+} in Cells*, ed. ASHLEY, C. C. & CAMPBELL, A. K., pp. 85–115. Amsterdam: Elsevier/North Holland.

SCARPA, A., BRINLEY, F. J. & DUBYAK, G. (1978). Antipyrylazo III, a 'middle range' Ca^2 metallochromic indicator. *Biochemistry*, N.Y. **17**, 1378–1386.

SCHNEIDER, M. F., RIOS, E. & KOVACS, L. (1981). Calcium transients and intramembrane charge movement in skeletal muscle. In *The Regulation of muscle Contraction: Excitation–Contraction Coupling*, ed. GRINNELL, A. D. & BRAZIER, M. A. B., pp. 131–142. New York: Academic Press, Inc.

THOMAS, M. V. (1979). Arsenazo III forms 2:1 complexes with Ca and 1:1 complexes with Mg under physiological conditions. *Biophys. J.* **25**, 541–548.

VERGARA, J., BEZANILLA, F. & SALZBERG, B. M. (1978). Nile Blue fluorescence signals from cut single muscle fibers under voltage or current clamp conditions. *J. gen. Physiol.* **72**, 775–800.